doi:10.1111/evo.12684

A molecular mechanism for the origin of a key evolutionary innovation, the bird beak and palate, revealed by an integrative approach to major transitions in vertebrate history

Bhart-Anjan S. Bhullar,[1,2,3,4,5] Zachary S. Morris,[1] Elizabeth M. Sefton,[1,6] Atalay Tok,[1] Masayoshi Tokita,[1] Bumjin Namkoong,[1] Jasmin Camacho,[1] David A. Burnham,[7] and Arhat Abzhanov[1,8,9,10]

[1]Department of Organismic and Evolutionary Biology, Harvard University, 16 Divinity Avenue, Cambridge, Massachusetts 02138

[2]Department of Organismal Biology and Anatomy, University of Chicago, 1027 E. 57th St., Anatomy 306, Chicago, Illinois 60637

[3]Department of Geology and Geophysics, Yale University, P.O. Box 208109, New Haven, Connecticut 06520

[4]Peabody Museum of Natural History, Yale University, P.O. Box 208109, New Haven, Connecticut 06520

[5]E-mail: bhart-anjan.bhullar@yale.edu

[6]Museum of Comparative Zoology, Harvard University, 26 Oxford Street, Cambridge, Massachusetts 02138

[7]Biodiversity Institute and Natural History Museum, University of Kansas, 1345 Jayhawk Boulevard, Lawrence, Kansas 66045

[8]Current address: Department of Life Sciences, Imperial College London, Silwood Park Campus Buckhurst Road, Ascot, Berkshire SL5 7PY, United Kingdom

[9]Natural History Museum, Cromwell Road, London SW7 5BD, United Kingdom

[10]E-mail: aabzhano@gmail.com

Received December 28, 2014
Accepted April 8, 2015

The avian beak is a key evolutionary innovation whose flexibility has permitted birds to diversify into a range of disparate ecological niches. We approached the problem of the mechanism behind this innovation using an approach bridging paleontology, comparative anatomy, and experimental developmental biology. First, we used fossil and extant data to show the beak is distinctive in consisting of fused premaxillae that are geometrically distinct from those of ancestral archosaurs. To elucidate underlying developmental mechanisms, we examined candidate gene expression domains in the embryonic face: the earlier frontonasal ectodermal zone (FEZ) and the later midfacial WNT-responsive region, in birds and several reptiles. This permitted the identification of an autapomorphic median gene expression region in Aves. To test the mechanism, we used inhibitors of both pathways to replicate in chicken the ancestral amniote expression. Altering the FEZ altered later WNT responsiveness to the ancestral pattern. Skeletal phenotypes from both types of experiments had premaxillae that clustered geometrically with ancestral fossil forms instead of beaked birds. The palatal region was also altered to a more ancestral phenotype. This is consistent with the fossil record and with the tight functional association of avian premaxillae and palate in forming a kinetic beak.

KEY WORDS: **Aves, cranial, development, macroevolution, morphology, novelty.**

EVOLUTION
INTERNATIONAL JOURNAL OF ORGANIC EVOLUTION

The long history of Vertebrata is marked by a series of morphological transitions, revealed by the fossil record, that seem to precede and in part enable the great radiations that occurred near the base of the major vertebrate clades (Romer and Parsons 1990). Such for instance is the appearance of limbs that preceded the radiation of tetrapods (Gillis et al. 2009; Shubin et al. 2009), of the uterus and placenta that preceded the radiation of therian mammals (Lynch et al. 2004, 2008, 2011), and of the head and brain that enabled the initial radiation of Vertebrata itself (Gans and Northcutt 1983; Northcutt 2011). These watershed changes are sometimes referred to as key evolutionary innovations (Heard and Hauser 1995). Their historical details must be sought in the comparative morphology of extant and fossil taxa, and their proximate mechanisms in alterations of embryonic development (Gilbert 2010). We undertook an investigation of a great anatomical transformation at the genesis of one of the most speciose vertebrate clades.

Comprising over 10,000 species, birds are among the most successful land vertebrates and much of their ecological expansion is intimately associated with the dramatic variation of their beaks (Gill 2006). Beak morphological diversity provides some of the most compelling evidence for evolution by natural selection (Darwin 1859; Grant and Grant 2008). The bird beak meets several criteria of a key evolutionary innovation (Hodges and Arnold 1995) as it appeared just before radiation into new adaptive zones (Simpson 1953) and an explosion of avian speciation and accompanying beak diversity and disparity followed a massive environmental cataclysm, the end-Cretaceous extinction event (Liem 1973; Mayr 2009; Jetz et al. 2012; Brusatte et al. 2014). The beak also represents a distinct functional and developmental module with respect to the remainder of the skull (Abzhanov et al. 2006, 2007; Mallarino et al. 2011; Wagner 2014).

Anatomically, the internal skeleton of the upper beak is composed of fused, elongated premaxillary bones; these are paired, small, and form the tip of the snout in ancestral reptiles (Figs. 1A and 3L). The remainder of the snout and much of the face in birds are truncated, a paedomorphic (Hanken and Wake 1993) condition with respect to ancestral archosaurs (Bhullar et al. 2012; Balanoff et al. 2013; Lee et al. 2014; Fig. 1A). Our previous work showed the beginning of the transition toward modern birds at the phylogenetic level of Ornithurae (Yanornithiformes; Fig. 1C), whose premaxillae are expanded beyond the paedomorphic condition displayed by more basal avialans (with respect to Aves) such as *Archaeopteryx* (O'Connor and Chiappe 2011; Bhullar et al. 2012; Zhou et al. 2013). However, although significant effort has been devoted to understanding the systematics of extant and extinct birds in the last two decades (Mayr and Clarke 2003; O'Connor and Zhou 2013), no previous studies have specifically traced the transformation of the avian rostral skeleton (though see Young et al. 2014).

Developmentally, the bird premaxilla forms from neural crest derived mesenchyme filling the frontonasal prominence in the middle of the face of early embryos (Noden 1978; Couly et al. 1993; Lee et al. 2004; Le Douarin et al. 2007; Wada et al. 2011). Two frontonasal signaling systems active at different times during embryonic development have been broadly hypothesized to be responsible for facial differences between the two distantly related and highly derived biomedical model amniotes, chickens, and mice. The first is the frontonasal ectodermal zone (FEZ), which is present in three-day-old chicken embryos (Hamburger–Hamilton stages 18–20) and is composed of dorsoventrally apposed expression domains of *Fibroblast growth factor 8* (*Fgf8*) and *Sonic hedgehog* (*Shh*; Hu et al. 2003). *Fgf8* is expressed in a wide medial domain across the dorsal side of the developing chicken face and it is dominant in the part of the frontonasal prominence that will generate the premaxillae (Fig. 2A). *Shh* is expressed in the ventral portion of the face and in the oral epithelium and its expression is linked by cross-regulatory interactions with that of *Fgf8* such that *Fgf8* expression predicts *Shh* expression ventral to it. (Hu et al. 2003).

The second signaling system implicated in bird-specific facial morphology is based on the WNT pathway, which is active in the frontonasal prominence for a period of time following the FEZ but preceding skeletogenesis (Brugmann et al. 2007). Earlier studies have indicated that expression of FEZ molecules varies across vertebrate species (focusing on mouse and chicken) and, in particular, have suggested that differences in *Shh* and WNT signaling could explain many important species- and clade-specific craniofacial features, such as facial width and fusion of facial primordia (Hu et al. 2003; Brugmann et al. 2007; Hu and Marcucio 2009b; Hödar et al. 2010; Reid et al. 2011; Compagnucci et al. 2013; Griffin et al. 2013; Hu and Albertson 2014; Parsons et al. 2014; Young et al. 2014). Detailed morphometrics of the embryos of a range of amniotes demonstrated the gradually diverging facial shapes of birds and nonavians (Young et al. 2014). However, these earlier reports did not phylogenetically map expression of *Fgf8* and the WNT signaling pathway or functionally test the roles of patterning differences generating in a way that replicated rigorously inferred ancestral patterns.

To address the evolutionary and developmental origin of the avian beak, we implemented the following research program, developed for studying large-scale evolutionary novelties: first, we traced the transformation of the distinctive avian facial skeleton in the fossil record using geometric morphometrics (Klingenberg 2011). We then attempted to determine developmental mechanisms behind the origin of the avian rostrum. We investigated potential developmental causes by examining candidate gene expression domains in several nonmodel reptiles and birds to phylogenetically polarize expression patterns, and then experimentally restored the inferred ancestral craniofacial expression patterns

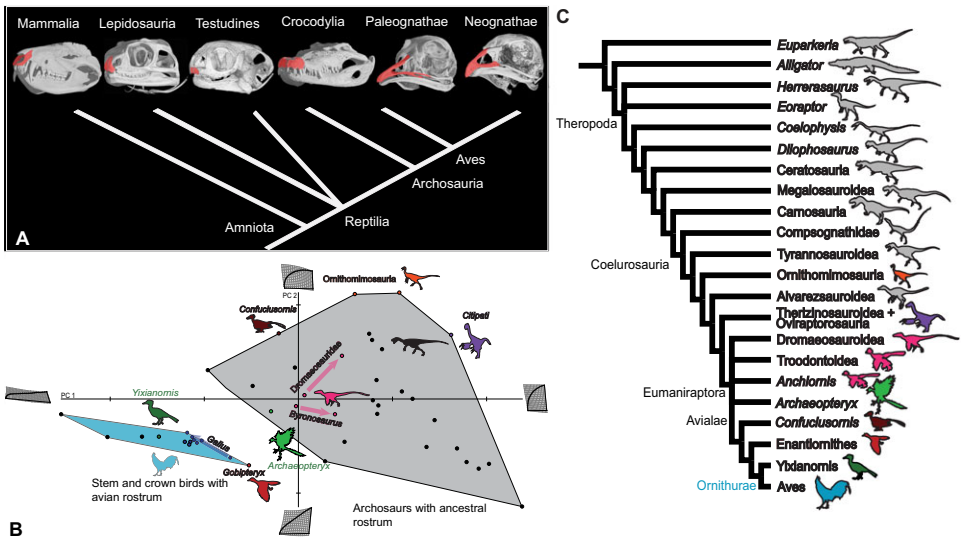

Figure 1. **The origin of the avian rostrum. (A) Amniote phylogeny showing major clades and configuration of the premaxillae. The avian rostrum is formed from autapomorphically fused, elongate premaxillae. Images from UTCT/Digimorph.org. (B) PCA plot of dorsal view of premaxilla with outline images of hypothetical extremes along each axis, set on deformation grids from average. Taxa with an avian rostrum, including the transitional form *Yixianornis* and adult and embryonic chickens (in dark blue) cluster away from the remaining archosaurs. *Gobipteryx* convergently evolved avian-like premaxillae. *Confuciusornis*, ornithomimosaurs, and some oviraptorosaurs (*Citipati* here) were toothless and probably had a rhamphotheca, both components of the definitive avian "beak," but premaxillary shape was not birdlike. Approximate ontogenetic trajectories are shown using arrows for dromaeosaurs generally, *Byronosaurus*, and *Gallus*. The two nonavian dinosaurs have longer, narrower premaxillae when younger; the bird has longer, narrower premaxillae when older. (C) Phylogeny of Archosauria plus *Euparkeria* showing major clades discussed in text. Modified after Bhullar et al. (2012).**

in developing chicken embryos. To validate the results of these functional experiments, we included the resultant cranial phenotypes in the broader geometric morphometric analysis, which contained ancestral snouted and bird-faced fossil forms, and found that, as predicted, premaxillae of the manipulated embryos closely corresponded to ancestral phenotypes, in particular those characteristic of primitive avialans.

Methods

An account of methods is provided in the Supporting Information.

Results

THE APPEARANCE OF THE AVIAN ROSTRUM IN THE FOSSIL RECORD

We conducted a principal component analysis (PCA) of shape variation in the dorsal view of the premaxilla of a range of extant and extinct archosaurs, focusing on the avian lineage and including embryos, juveniles, and adults (Fig. 1B, C). The images employed in our study included new high-resolution microcomputed tomography (μCT) scans of several exceptionally preserved specimens of the near-crown ornithurines (Clarke 2004) *Hesperornis* and *Parahesperornis* (Supporting Information) and embryos of birds and crocodylians (Fig. 6). Our choice to use dorsal view was influenced by two factors. First, many crucial stem avians are preserved two-dimensionally, crushed flat upon slabs of shale or limestone. Second, the candidate genes we examined vary phylogenetically in their expression primarily in a mediolateral way, and thus we expected mediolateral phenotypic differences in experimental individuals that would be captured only in dorsal view.

Premaxillary landmarks are depicted in Figure 3L. Their descriptions follow: (1) anterior tip of premaxilla, (2–23) sliding semilandmarks describing curve along lateral edge of premaxilla between (1) and (24), (24) posteriormost extent of maxillary process of premaxilla, dorsal exposure, (25) point along the midline, even with (24) along anteroposterior axis. Palatine landmarks are depicted in Figure 3M. Their descriptions follow: (1) anterior tip of lateral/maxillary process of palatine, (2) deepest point of choanal margin, (3) anterior tip of medial/vomerine process of palatine, (4) posterolateral corner or inflection of body of palatine, (5) posterior tip of pterygoid process of palatine.

The first two principal components (PCs) of the PCA explained 68.24 and 16.73% of the variation found in the sample, respectively; all others explained less than 8% (Fig. 1B). The first of the two principal axes (PC 1) accounted for the overall proportions of the premaxilla, changing from short and broad to long

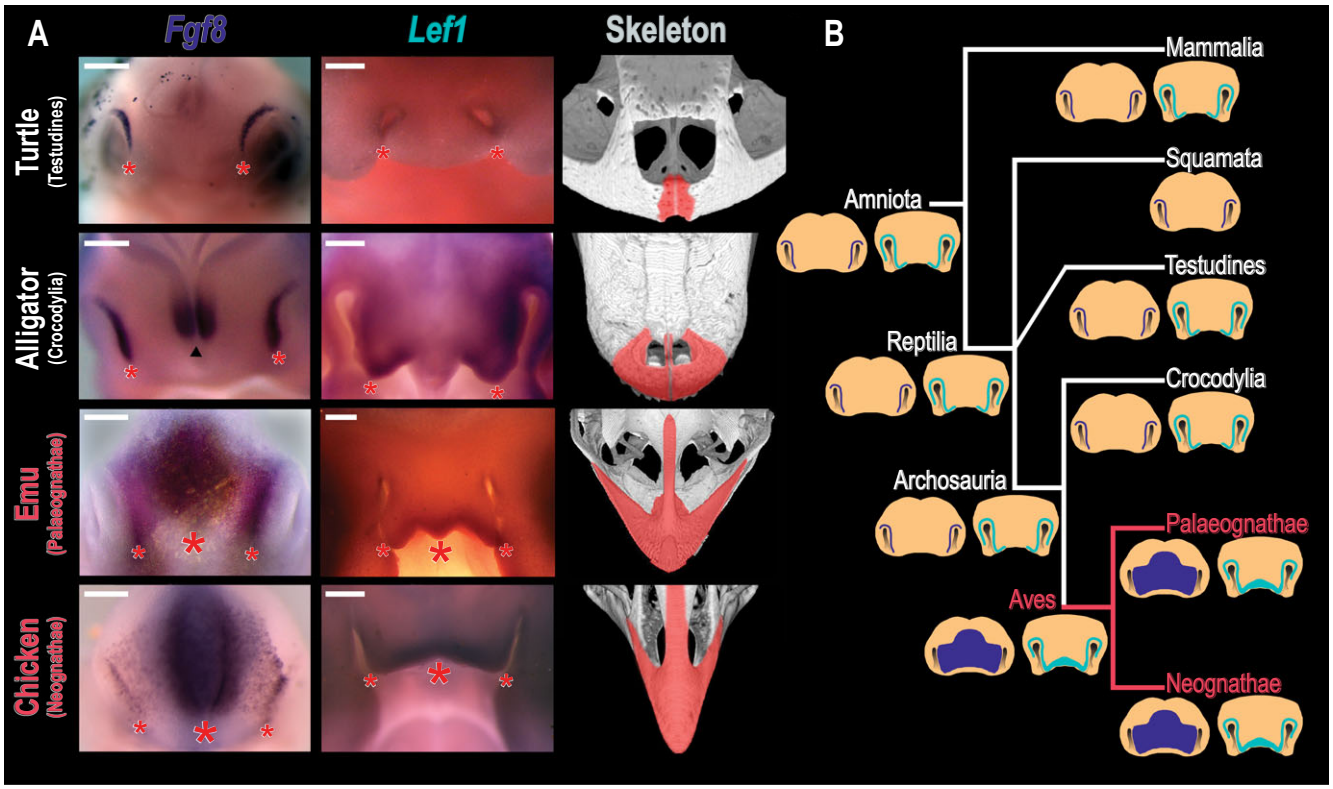

Figure 2. Expression of facial patterning genes across amniotes. (A) Expression of *Fgf8* and *Lef1* and adult skeletal phenotypes in reptiles, showing ancestral paired gene expression preceding small, paired premaxillae in turtles and alligators and median zone of expression preceding elongate, fused premaxillae in birds. Skeletal images from UTCT/digimorph.org. (B) Amniote phylogeny with data on facial patterning gene expression and inferred ancestral states shown. Dark blue: *Fgf8*. Light blue: *Lef1*. The median expression zone is an autapomorphy of birds correlated with the presence of the avian rostrum. Scale bars 500 μm.

and narrow. The second principal axis (PC 2) accounted for the curvature of the lateral edge of the premaxilla. A statistical test of phylogenetic structure in the data for all PCs strongly rejected the null hypothesis of no structure ($P < 0.0001$; see Supporting Information and Fig. S2A).

Adult and embryonic birds and some stem birds were separated from the ancestral forms along PC 1 in having relatively long and narrow premaxillae, and along PC 2 in having relatively straight-edged premaxillae (Fig. 1B). *Yixianornis*, the basal-most taxon with an enlarged premaxilla as detected by our earlier study (Bhullar et al. 2012), *Archaeorhynchus*, an ornithurine with a modern-looking rostral configuration but incomplete fusion of the premaxilla, and *Hesperornis*, the closest sister taxon to crown Aves with a well-preserved rostrum, all fell into the avian-faced cluster. *Yixianornis* is described (Clarke et al. 2006) as having premaxillae fused in the front (rostrally) but not at the back. The anterior fused region is also toothless, with some rudimentary teeth dotting the back of the bone. Although not commented upon as such in published descriptions, in our view this morphology represents a plausible transitional state toward the fused, toothless rostrum of crown Aves. Thus, provisionally we can state that the major shape transformation leading to an elongate rostrum homologous to that of crown-clade birds had occurred by the Ornithurae node.

Three ontogenetic sequences are included in the analyses—one composite ontogeny consisting of the juvenile dromaeosaur *Bambiraptor* and the adult *Velociraptor*, one for the troodontid *Byronosaurus*, and one for the chicken *Gallus* (Fig. 1B, arrows). During ontogeny, the nonavian dinosaurs move farther from the avian condition along PC 1, becoming shorter and broader. The earlier ontogenetic stages are the more birdlike. This suggests that a somewhat long and narrow premaxilla is in fact a juvenile feature and that a portion of the transformation to the avian premaxillary shape (although not the sharp break represented by the gap between the beaked and nonbeaked clusters) perhaps owed to paedomorphosis, as did the transformation of much of the remainder of the avian skull (Bhullar et al. 2012). However, chickens move in the opposite direction, the premaxillae becoming longer and narrower during ontogeny. This suggests that once the transformation to the beak occurred, a different modality of growth began to control ontogenetic change in premaxillary shape.

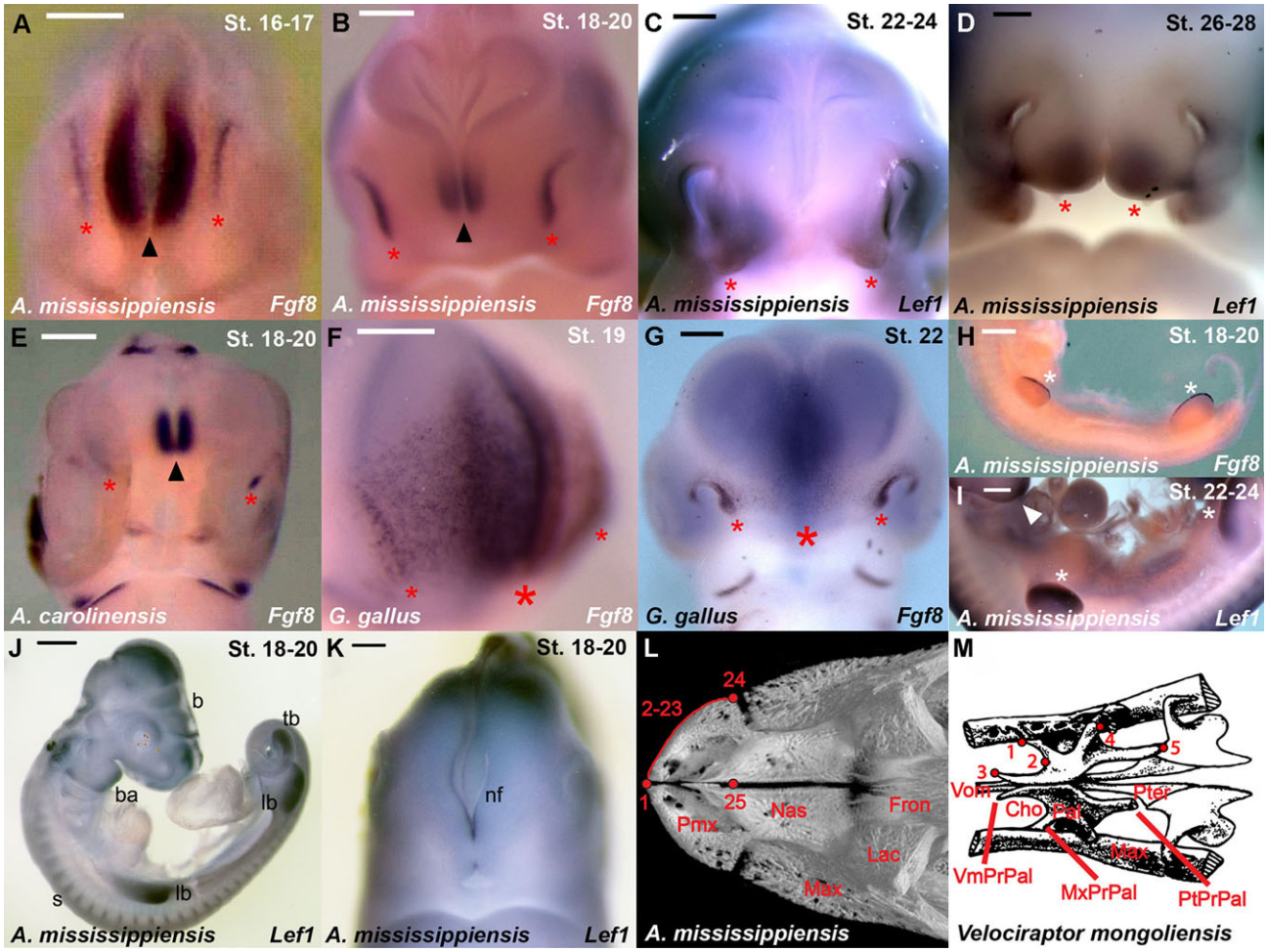

Figure 3. Additional gene expression data and landmark positions. (A) Expression of *Fgf8* (red stars) in HH 16–17 equivalent alligator, showing paired ancestral amniote epithelial expression even at an early stage; arrowhead denotes expression in brain. (B) Expression of *Fgf8* (red stars) in HH 18–20 equivalent alligator, showing paired expression with arrowhead denoting expression in brain. (C) Expression of *Lef1* in HH 22–24 equivalent alligator, showing ancestral amniote paired expression with no midline expression. (D) Expression of *Lef1* in HH 26–28 equivalent alligator, showing continued absence of midline expression in region where birds have downgrowth of the presumptive beak apex (see Fig. 2A). Eventually the suture between premaxillae will form here. (E) Expression of *Fgf8* in HH 18–20 equivalent anole lizard, showing ancestral amniote paired expression (stars) with arrowhead denoting brain expression. (F) Expression of *Fgf8* in HH 19 chicken, showing broad median swath of expression unique to birds. (G) Expression of *Fgf8* in HH 22 chicken, showing continuing midline expression at relatively late stage. (H) expression of *Fgf8* in body of HH 18–20 equivalent alligator (left lateral, flipped) showing expression in apical ectodermal ridges (stars). (I) Expression pattern of *Lef1* in body of HH 22–24 equivalent alligator (right lateral) showing mRNA accumulation in limbs (stars), somites, and branchial arches (arrowhead). (J) Expression of *Lef1* in HH 18–20 equivalent alligator showing distinct activity in the expected regions of the brain (b), branchial arches (ba), limb buds (lb), tail bud (tb), and somites (s). (K) Detail of head of HH 18–20 equivalent alligator stained for *Lef1* expression. There is no discernible expression in the anterior facial mesenchyme; thus WNT activity temporally follows FGF activity in the front of the face. Expression is clearly visible in the neural folds (nf) of the forebrain. (L) Premaxillary landmarks and facial anatomy on alligator rostrum in dorsal view. Pmx, premaxilla; Nas, nasal; Max, maxilla; Lac, lacrimal. (M) Palatine landmarks and palatal anatomy in *Velociraptor mongoliensis* modified after(Barsbold and Osmólska 1999). Vom: Vomer. Pal: Palatine. Pter: Pterygoid. Max: Maxilla. Cho: Choanal margin. VmPrPal: Vomerine process of palatine. MxPrPal: Maxillary process of palatine. PtPrPal: Pterygoid process of palatine. Scale bars 500 μm (a-g, j) and 1 mm (h-i, k).

Ornithomimosaurs and oviraptorosaurs are two dinosaurian lineages that independently acquired a toothless, probably rhamphotheca-covered rostrum. Despite overall similarity with bird beaks, premaxillary shapes of these taxa grouped with those of more conservative archosaurs (Fig. 1B). Within avialae, it has been suggested that tooth reduction and loss, premaxillary fusion, and other characteristic components of the "beak" phenotype appeared multiple times during avian evolution (Zhou and Li 2010).

For instance, *Confuciusornis* has a toothless rostrum with partially fused premaxillae. However, although its premaxillae are toothless and partially fused in their middle region, their short, broad, laterally rounded shape is distinct from those of modern birds and clusters with the more conservative nonavian archosaurs (Fig. 1B). The aberrant enantiornithine *Gobipteryx*, on the other hand, appears to have fused premaxillae and evolved a crown bird like premaxillary shape as its rostrum clusters with beaked birds (Fig. 1B). Thus, various degrees of similarity to a birdlike premaxillary skeleton have appeared convergently in extinct avialan lineages. Although these phenotypes are suggestive, it is impossible to infer and compare molecular mechanisms in completely extinct lineages using phylogenetic bracketing.

EXPRESSION OF CANDIDATE GENES IN BIRDS AND OUTGROUPS

It has been shown (Hu and Marcucio 2009b; Griffin et al. 2013) that in mice at the phylotypic stage (as identified in our work by the onset of facial fusion) the genes that define the FEZ are expressed in the facial epithelium—the region of ectoderm that will form the skin of the face and that will signal to the underlying mesenchyme to pattern the dermal bones and connective tissue—in a paired pattern as thin lines of expression arcing over the nasal pits, likely established by signaling from nasal placodes. In chicken embryos at developmental stages HH 18–20, on the other hand, they are expressed not only around the nasal pits, but also in a broad ectodermal median domain between them, including a tall oval-shaped patch in the center of the embryonic face ($n = 4$, Fig. 2A).

To phylogenetically polarize FEZ configuration and to pinpoint the developmental transformation, we cloned *Fgf8* from emu, a paleognath bird, the sister group to the remainder of Aves, and alligator, representing Crocodylia, the extant sister taxon to birds. We were also able to examine FGF expression in an *Anolis* lizard, representing Squamata as a further reptilian outgroup, and FGF and WNT signaling in turtles (*Trachemys scripta*), whose phylogenetic position among reptiles remains uncertain. Emu ($n = 4$, Fig. 2A) has a chicken-like median swath of epithelial expression with a large oval-shaped domain in the center at stages equivalent to chicken stages HH 18–20, and part of the median expression zone persists to the later stages equivalent to HH 21–22, which is similar to what is observed in chicken (Fig. 3F–G). Alligator ($n = 7$), lizard ($n = 2$), and turtle ($n = 1$), on the other hand, show no median ectodermal expression at the phylotypic stage and all instead have narrow mouse-like paired expression domains in the vicinity of the nasal pits throughout early development (Figs. 2A, B and 3A, B, E).

WNT pathway activity, which occurs later in embryogenesis (Brugmann et al. 2007) and is not present in the anterior face at the phylotypic stage as indicated by the expression of the WNT pathway direct target gene *Lef1* (Hödar et al. 2010; Fig. 3J, K—note lack of expression in face of alligators at phylotypic stage), is, like *Fgf8*, paired in the embryonic face of mice, but found in a median position in chickens ($n = 6$, Fig. 2A). We cloned the *Lef1* homolog from emu and alligator and established that emu shows a strong chicken-like median expression pattern ($n = 3$, Fig. 2A), whereas expression of this WNT signaling marker in alligator ($n = 4$) and turtle ($n = 1$) embryonic faces is again mouse-like and paired with no median expression detected (Figs. 2A and 3C, D). The midline facial cleft correlating with the absence of medial WNT expression persists into later stages in alligator embryos ($n = 3$, Fig. 3D). This is suggestive in that adult alligators retain here a midline suture between their premaxillae, but further work is required to determine whether there is a direct relationship between the embryonic midline cleft and the complex processes of skeletal tissue formation that result in a suture(Warren et al. 2003). Birds, on the other hand, do not show this median cleft and instead develop a convex outgrowth in the middle of the FNP, as shown in the later-stage emu in Figure 2A. Turtles have unusually small premaxillae among the amniotes sampled (Fig. 1A) and already display a relatively small frontonasal prominence at this early stage, suggesting perhaps that comparatively less neural crest is recruited to the frontonasal prominence or that less proliferation occurs here.

Parsimony analysis concluded that the ancestral amniote condition is the mouse-like paired expression domains for both *Fgf8* (as part of the FEZ) and for the activated WNT pathway later in development (Fig. 2B). A novel median zone of expression and activity in both of these signaling pathways must have originated along the stem of Aves and correlates with the presence of an upper beak dominated by fused and enlarged premaxillae.

FUNCTIONAL TEST BY RESTORATION OF ANCESTRAL PATTERNING

There is a rich literature concerning early craniofacial patterning and potential mechanisms of interspecies differences. Functional validation of these purported differences has thus far been limited to a two-taxon mouse versus chick comparison, which is of course not phylogenetically polarized. Previously published functional tests demonstrated that a portion of the mouse FEZ grafted off-center beside the native FEZ causes secondary outgrowth in the chicken face and that unilateral or midline inhibition of *Fgf8* using high concentrations of the inhibitor su5402 (i.e., near total suppression of the FEZ) results in a phenotype lacking most of the rostral bones on the affected side of the face or the entire face, respectively (Hu et al. 2003; Abzhanov et al. 2007; Brugmann et al. 2007; Hu and Marcucio 2009a,b, 2012). A series of suggestive results also demonstrated that reducing WNT activity in the chick FNP broadly could shrink the structure (but lack of specific mid-FNP induction prevented the generation of an ancestral

phenotype; Brugmann et al. 2007); and that unilateral FNP/maxillary clefts can be induced by alteration of facial signaling (Young et al. 2014). However, specific inhibition of expression in the central portion alone of embryonic bird FNPs to replicate an inferred ancestral pattern has not been attempted (in part because no ancestral pattern could be inferred without expression data from the taxa we present here), and many of the previous studies did not examine late-stage skeletal phenotypes, instead looking only at the shapes of the preskeletal embryonic primordia.

To more accurately replicate the ancestral paired amniote expression patterns of *Fgf8* and WNT in chicken embryos, we used low concentrations of two different small-molecule inhibitors of FGF activity (respectively, targeting FGF receptor 1 and MAPK) and two specific inhibitors targeting different parts of the canonical WNT pathway (see Supporting Information for details) at the appropriate embryonic stages to block the bird-specific medial domains of these molecules and reestablish the ancestral condition dominated by the paired lateral domains. To this end, a bead soaked with the inhibitors was implanted in the middle of the embryonic face at stage HH18–20 (E3) for the FEZ and HH24 (E5) for the WNT pathway (Fig. 4A).

Multiple experimental embryos with median inhibition of FGF activity were collected at HH stage 24 (E5) to determine the effect on the WNT pathway. In most (five of eight) of these embryos, *Lef1* expression was found in paired expression domains to varying degrees, progressively resembling the ancestral condition (Fig. 4B). Moreover, alligator embryos with the ancestral paired expression, control embryos, and experimental embryos were collected and sectioned coronally to examine cell death (using a TUNEL kit, Life Technologies: Carlsbad, CA) and proliferation (using antiphosphohistone H3 antibody, Cell Signaling Technology: Danvers, MA) in the FNP. Cell death is a potential side effect of some of the small molecular inhibitors used. We found (Fig. S1) that the mesenchymal tissue in the distal FNP of experimental embryos was present, not degenerated, and free of excessive cell death. This is consistent with the presence of midline tissue in the E14 skeletal phenotypes we sectioned as described below. Proliferation was present generally at the leading edge of the growing FNP.

Near-hatching skeletal phenotypes of both FGF- and WNT-inhibited experimental individuals were similar to each other and both strikingly resembled ancestral archosaurian forms in having abbreviated, rounded, and partially or fully paired premaxillae (42/67 late-surviving experimental embryos vs. 0/56 controls; Fig. 4A, B, Fig. S3, and Supporting Information). Embryos with strong phenotypes displayed complete separation of the premaxillae with a suture-like division between them. Bilateral rostral structures were not duplicated, obviating concern that a simple pairing of the snout had occurred. Embryos with mild phenotypes (Fig. 4B) showed a small amount of fusion where the premaxillae normally begin to fuse at HH 39–40 (E13–14). In normal chicken embryos this continues until the premaxillae are fully fused by HH 41 (E15). However, in the manipulated embryos, no further median ossification occurred by the near-hatching stage 45–46 (E19–20), suggesting that the lack of fusion is not a simple delay and instead represents a true loss of premaxillary fusion.

To further investigate the skeletal phenotypes, we sectioned an experimental embryo at stage HH40 (E14) and a stage-matched control embryo and examined expression of early and late skeletogenic markers. At this stage the premaxillae are fusing by dorsomedial addition of bone, a process characterized by interdigitating bone spicules and a forming periosteum visible between the premaxillae of the control embryo, whereas the premaxillae of the experimental embryo remained separate with no incipient bone development bridging them (Fig. 4C). Strong expression of the skeletal markers *Runx2* (early) and *Osteopontin* (late) was detected in the fusion zone of the control embryo, but not in the unossified area between the two premaxillae in the experimental animal. Likewise, the early osteogenic marker *Col I* was weakly expressed all around the periosteum and there was strong expression in the fusion zone of the control embryo, marking an area of future active osteogenesis. In contrast, no *Col I* expression was detected between the premaxillae in the experimental embryo, indicating the removal of the fusion zone.

In addition to the premaxillary bone phenotype, the palates of all but one of the phenotype-positive experimental embryos also showed an altered and more ancestral phenotype. The palatine bone in ancestral archosaurs (Figs. 3M and 4D) bears a medial vomerine process and a lateral maxillary process, both relatively short, and between them stretches a broad triangular lamina of bone (Colbert 1989). The maxillary process is directed outward and is sutured to the maxilla (Barsbold and Osmólska 1999). In birds, however, the vomerine process is short, the lamina is reduced, and the maxillary process is extremely long and runs straight forward to meet the premaxilla, bypassing the maxilla (Fig. 4D). This is the case even in paleognaths with their famously more ancestral palate, and is true in the earliest chicken embryos that have ossified palatines (Fig. S4). The palatines of the experimental embryos had ancestral phenotypes featuring an extensive lamina and a primitively short, outwardly directed maxillary process terminating at the maxilla (Fig. 4D): a shape change evidently caused by a fundamental patterning difference related to the FEZ instead of simple stunting of growth, considering that, as noted above, the normal bird palatine never in its development resembles the ancestral structure in proportions or in the direction and termination of the maxillary process.

Apparent pleiotropic effects of the FGF and WNT pathways on both the premaxillae and the palatines are also consistent with our analysis of data from μCT scans of the palate of *Hesperornis*, the first stem-group bird with a completely transformed upper

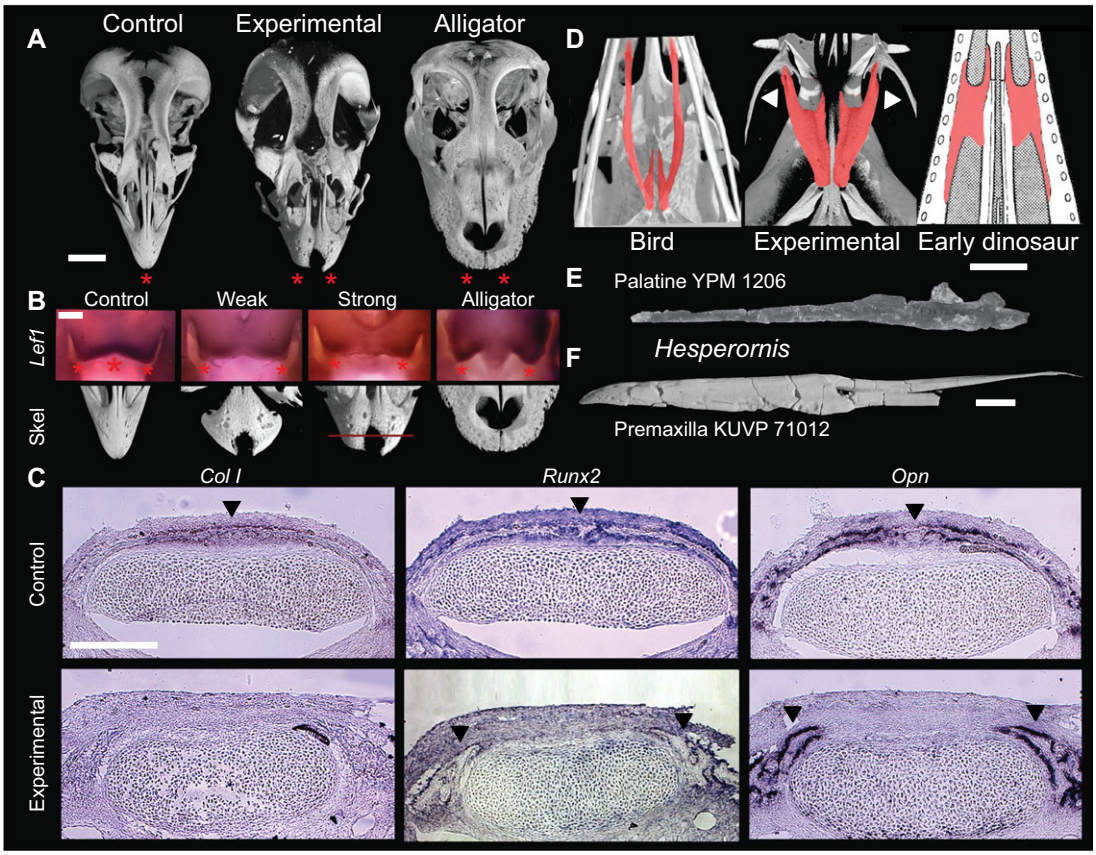

Figure 4. Experimental restoration of predicted ancestral expression. (A) Control chicken, experimental chicken, and alligator, showing ancestral paired, abbreviated, rounded premaxillae in experimental animal. (B) *Lef1* expression (red stars) in control chicken, experimentals, and alligator, and corresponding premaxillary phenotypes. In the experimental *Fgf8*-inhibited animals, *Lef1* expression is more paired like the ancestral state represented by the alligator. (C) Expression of skeletal and skeletogenic markers in control and experimental embryos; level of section shown in red on strong phenotype skeleton image. The median fusion zone that unites the two premaxillae in control chickens (upper arrowheads) is absent in the experimentals, which instead have paired ossifications (lower arrowheads). (D) Palatal morphology in normal chicken (UTCT/digimorph.org), experimental embryo, and ancestral archosaur (after Colbert 1989). The palatine in the experimental embryo resembles the ancestral form in having a short maxillary process ending at the maxilla (arrowheads) and an extensive triangular lamina between processes. (E) The palatine of the near-crown stem bird *Hesperornis regalis* YPM (Yale Peabody Museum) 1206. This element is essentially identical to that of crown-clade birds in its overall configuration. (F) The fused premaxillae of the near-crown stem bird *Hesperornis regalis* KUVP (University of Kansas) 71012. Like the palatine, this element essentially represents a modern avian configuration. Scale bars 1 cm (a, e, f), 500 μm (b), 100 μm (c).

beak. In correlation with its modern beak (Marsh 1880), *Hesperornis* has a fully modern bird palatine (Fig. 4E, F). However, the nonavian theropod *Gobipteryx* has both modern birdlike premaxillae and unmodified primitive palatines. This suggests that these structures became genetically linked within the avian lineage sometime after *Gobipteryx* split from the avian stem, but before the divergence of *Hesperornis* and modern birds.

MORPHOMETRIC ANALYSES OF THE EXPERIMENTAL PHENOTYPES

To quantitatively investigate whether our experiments indeed transformed premaxillary shape to the ancestral condition, we included premaxillae of 22 manipulated embryos with phenotypes harvested near hatching (E18–20) in the same morphometric analysis that generated the original hypothesis of rostral transformation. Although control embryos and experimental embryos showing near normal phenotypes clustered with forms possessing an avian rostrum (which includes adult chickens and other modern birds), all of the embryos with more pronounced phenotypes fell outside of the cluster of beaked birds and most of them instead clustered with more conservative archosaurs, suggesting that the ancestral snout developmental pattern and anatomy were indeed successfully resurrected (Fig. 5A).

To better understand the palatine phenotype in treated embryos, we also assembled and morphometrically examined

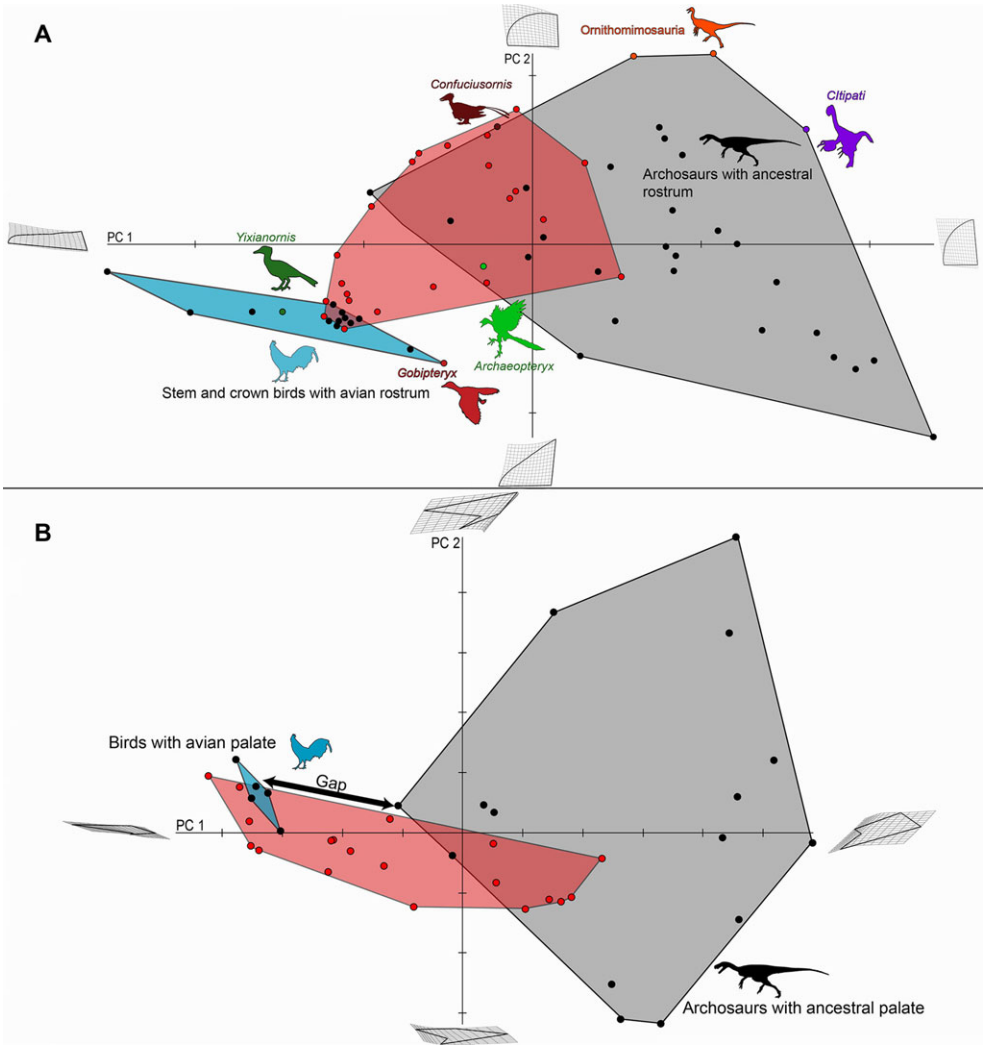

Figure 5. **Morphometric analysis of experimental embryos. (A) PCA of experimental premaxillae showing that the experimentals (in red) partially overlap the ancestral archosaurian morphospace. (B) PCA of experimental palatines showing that the experimentals (in red) fill the gap between crown-group birds and more ancestral archosaurs and overlap the nonavialan ancestral archosaur morphospace. We predict that as early avialan palatines become better known, the fossils will occupy the gap spanned by the experimental phenotypes.**

archosaurian palatine bones (Fig. 5B). Palates are poorly preserved in virtually all stem avialans, although we were able to add new data from our μCT scans of *Hesperornis* and *Parahesperornis* skulls (see Supporting Information). Because of the palatine's complicated shape, the resultant PCs were relatively complex. However, there was significant phylogenetic structure to the data ($P < 0.0001$, see Supporting Information and Fig. S2B), and the most basal archosaurs with respect to birds clustered in an adults-only analysis away from birds and more crown ward nonavian dinosaurs. Birds, including *Hesperornis*, clustered far from other archosaurs. A large gap between the birdlike and non-birdlike clusters presumably represents missing transitional forms among early avialans. The experimental embryos bridged this gap and overlapped the nonbird snouted archosaur cluster (Fig. 5B). Thus, we propose that the experimental embryonic phenotypes actually predict the morphology of yet undiscovered early avialan palatines and that new fossils will eventually be found that will show a gradual morphological transition toward modern birds. Despite the complexity of the pleiotropic linkage between beak and palatine noted above, a partial least squares analysis, including experimental embryos, found that premaxilla and palatine shapes were significantly correlated ($P < 0.001$ in permutation test against null hypothesis of independence, *RV* coefficient 0.3956, see Supporting Information).

Discussion

Major evolutionary transitions involving the origin of novel structures, with far-reaching implications for diversity and differentiation, are well-documented in the fossil record (Carroll

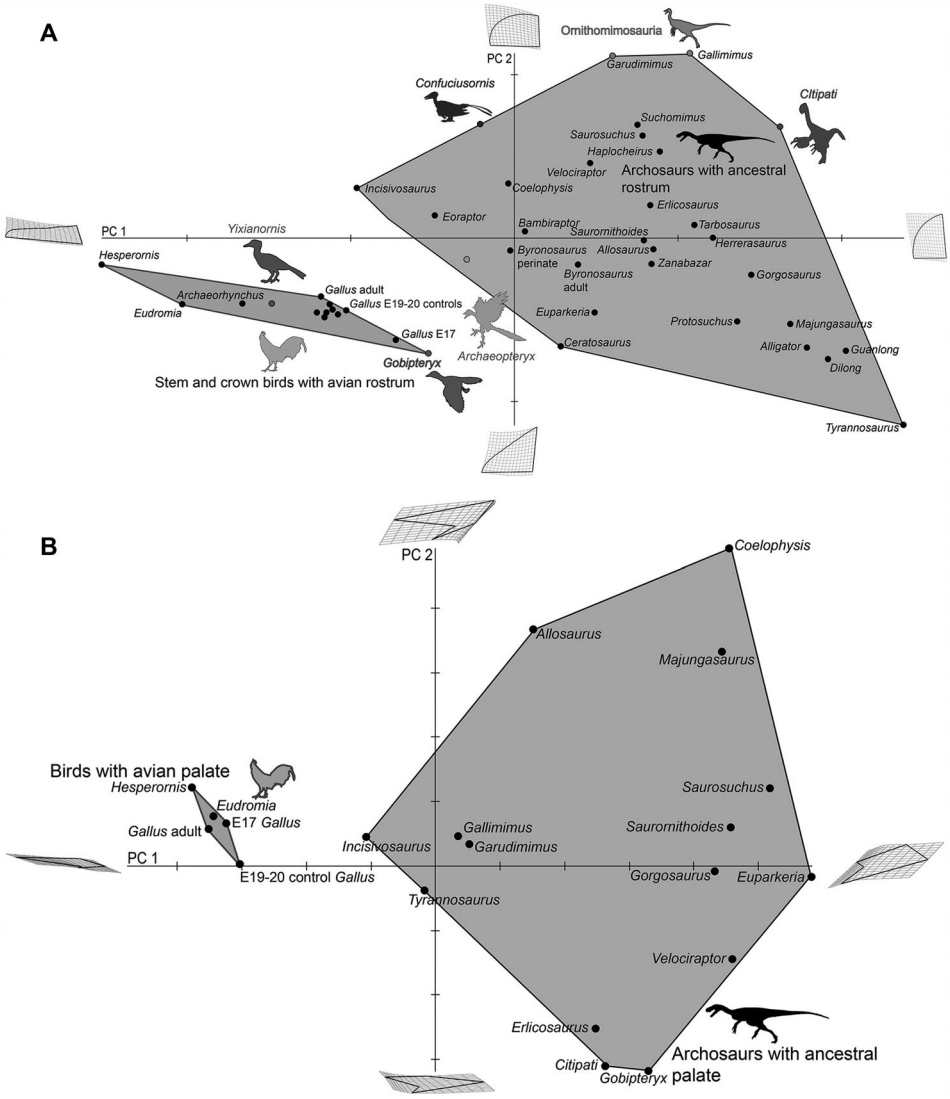

Figure 6. **Labeled morphometric plots. (A) Premaxilla. (B) Palatine.**

1988). Despite this extensive historical record, the molecular mechanisms of large-scale innovation and novelty have seldom been elucidated (Wagner and Lynch 2010). Here, we have shown that a relatively minor—though novel—additional region of gene expression at a sufficiently early stage can precipitate changes that result in a dramatic morphological transition of two distinct skeletal structures. We submit here that the phylogenetic distribution of gene expression suggests a role for FGF and WNT in the FNP in producing the distinct facial morphology of birds. We acknowledge, however, that the transition to the avian rostrum was undoubtedly complex—as shown by multiple transitions to a premaxilla with some bird beak like features in the fossil record. The results reported here represent one part of a manifold transition. Additionally, the characterization of the beak as a key evolutionary innovation is made more complex because its components were assembled over a longer period of time than that represented by the proximal stem of Aves—a caveat that applies to many such transformations or putative innovations (Donoghue 2005). However, the abrupt geometric gap between nonbeaked archosaurs and birds and stem birds with beaks may suggest a rapid, comparatively saltational transformation. The difference in ontogenetic trajectories of shape change between nonbeaked forms, in which the premaxilla becomes shorter and broader with time, and beaked forms, in which it becomes longer and narrower, also suggests a discontinuous distinctiveness to the beak.

The precise selective pressures that operated on the beak after its initial appearance are unknowable with certainty, but a series of careful, broadly comparative behavioral and functional morphological studies on the use of the avian feeding apparatus in paleognaths and conservative neognaths would make inroads

toward inferring the set of functions associated with the ancestral beak and therefore, indirectly, perhaps what environmental pressures led to the selection which resulted in its persistence and continued elaboration.

We have generated a hypothesis regarding a large-scale evolutionary event, the origin of modern birds (class Aves) with their distinctive facial skeleton, using the fossil record; formulated the potential developmental causes of the dramatic facial transformation using comparative embryological techniques; directly tested candidate molecular mechanisms, the medial FGF and WNT signaling centers, using functional experiments on developing bird embryos; and, finally, compared the resultant phenotypes back to the fossils. Similar progressions from morphology to development have worked well in the past to uncover mechanisms for small-scale evolutionary changes in various groups of animals, including birds (Abzhanov et al. 2004, 2006; Shapiro et al. 2004; Chan et al. 2010; Mallarino et al. 2011; Mallarino and Abzhanov 2012). The approach we demonstrate here, which explicitly "closes the circle" by including laboratory-generated phenotypes in the same analysis as fossil forms, can serve as a model for future investigations of macroevolutionary transformations inferred from the rock record. One of the most important aspects of the current approach is the recognition that evolutionary developmental transitions are single historical events. Thus, functional tests should be constrained by inferred ancestral states of gene expression or other developmental processes on both sides of the major anatomical transformation. This stands opposed to a blind search for phenocopies that merely resemble various morphologies. Undoubtedly in most cases there are many potential mechanisms that generate similar morphological shifts to a historical transition, but only one of these actually was responsible for the transformation. The precise historical mechanism is discoverable if embryonic material is available from extant taxa on both sides of the change.

Several insights into craniofacial developmental genetics also emerge from this work, including the downstream position of WNT pathway relative to FGF8 signal in early facial patterning, and the pleiotropy by which early midfacial signaling centers pattern both the premaxilla and much of the palate. Our observation of multiple morphological effects resulting from a single developmental change has implications for morphological systematics and modeling of morphological character evolution, which generally assume character independence (Patterson 1982; Hennig 1999). The goal of constructing a probability-based model for even simple anatomical structures based on the underlying genetics of development is still in the future (Clarke and Middleton 2008; Klingenberg 2008), but phylogenetically informed developmental studies aimed at a deeper understanding of roles for evolving developmental pathways move it incrementally closer to reality.

In addition, we have shown that just as the fossil record can provide developmental hypotheses, graded phenotypes resulting from restoration of the inferred ancestral developmental patterns can, in return, predict undiscovered transitional morphologies in the fossil record. For instance, we expect that stem avian palatines, as they are discovered and described, will resemble the gap-bridging palatal phenotypes we experimentally generated in chicken embryos.

Finally, the pleiotropic association of premaxillary fusion and shape transformation with palatine shape transformation demonstrates how changes in both of these structures can simultaneously contribute to the definitive avian beak. It may be significant that the loss of connection with the maxilla streamlines the palatine and makes the entire beak unit less integrated with the rest of the upper jaw, allowing for a more modular and flexible arrangement. The significance of such integrated changes remains to be rigorously investigated. The palatal transformation also frees the upper beak to move relative to the skull as part of the characteristic avian kinetic jaw mechanism (Gussekloo and Bout 2005). The set of transformations affecting the avian feeding apparatus, which apparently occurred at the same node or at very closely spaced nodes in the avialan tree, suggests an integrated morphofunctional complex like that long posited to have arisen in the form of multiple related anatomical transformations at the base of Mammalia (Crompton and Parker 1978). Precision tip gripping combined with kinesis, a novel avian jaw function, could ultimately have permitted the complete loss of teeth and the final transformations toward the face of living birds.

ACKNOWLEDGMENTS

We thank R. M. Elsey and colleagues at the Rockefeller Wildlife Refuge, Louisiana Department of Wildlife and Fisheries for helping us to obtain alligator embryos, D. D. Mares for assistance with emu embryos, J. A. Gauthier, C. A. Norris, and D. Brinkman for access to the YPM *Hesperornis* specimens, L. D. Martin and D. A. Burnham for access to the KU *Hesperornis* specimens, T. J. Sanger and J. B. Losos for assistance in obtaining the *Anolis* material. Moreover, T. J. Sanger assisted in initial cloning of *Fgf8* and *Shh* and O. Weeks provided primers for alligator *Lef1*. M. Fox photographed the Yale *Hesperornis* palatine. C. J. Tabin, S. V. Edwards, and J. B. Losos provided comments that improved the manuscript. The authors declare no conflicts of interest. B-ASB was partially funded by National Science Foundation dissertation improvement grant 1110564. Additional funding to B-ASB was provided by the University of Chicago, Yale University, the American Ornithologists' Union Research Award, the American Museum of Natural History Frank M. Chapman Memorial Fund Grant, and the Harvard Museum of Comparative Zoology Ernst Mayr Travel Grant in Animal Systematics. AA was funded by a Templeton Foundation (FQEB) grant and National Science Foundation grant IOS-1257122. B-ASB conceived and planned the study, collected embryos, performed experiments, and wrote the manuscript. ZSM helped to plan the study, collected embryos, performed experiments, and helped to write the manuscript. EMS performed experiments and helped to write the manuscript. AT, MT, BN, and JC performed experiments. AA conceived and planned the study, collected embryos, and wrote the manuscript.

LITERATURE CITED

Abzhanov, A., M. Protas, B. R. Grant, P. R. Grant, and C. J. Tabin. 2004. Bmp4 and morphological variation of beaks in Darwin's finches science 305:1462–1465.

Abzhanov, A., W. P. Kuo, C. Hartmann, B. R. Grant, P. R. Grant, and C. J. Tabin. 2006. The calmodulin pathway and evolution of elongated beak morphology in Darwin's finches. Nature 442:563–567.

Abzhanov, A., D. R. Cordero, J. Sen, C. J. Tabin, and J. A. Helms. 2007. Cross-regulatory interactions between Fgf8 and Shh in the avian frontonasal prominence. Congenit. Anom. 47:136–148.

Balanoff, A. M., G. S. Bever, T. B. Rowe, and M. A. Norell. 2013. Evolutionary origins of the avian brain. Nature 501:93–96.

Barsbold, R., and H. Osmólska. 1999. The skull of *Velociraptor* (Theropoda) from the Late Cretaceous of Mongolia. Acta Palaeontol. Pol. 44:189–219.

Bhullar, B.-A. S., J. Marugan-Lobon, F. Racimo, G. S. Bever, T. B. Rowe, M. A. Norell, and A. Abzhanov. 2012. Birds have paedomorphic dinosaur skulls. Nature 487:223–226.

Brugmann, S. A., L. H. Goodnough, A. Gregorieff, P. Leucht, D. ten Berge, C. Fuerer, H. Clevers, R. Nusse, and J. A. Helms. 2007. Wnt signaling mediates regional specification in the vertebrate face. Development 134:3283–3295.

Brusatte, S. L., G. T. Lloyd, S. C. Wang, and M. A. Norell. 2014. Gradual assembly of avian body plan culminated in rapid rates of evolution across the dinosaur-bird transition. Curr. Biol. 24:2386–2392.

Carroll, R. 1988. Vertebrate paleontology and evolution. W. H. Freeman and Company, New York.

Chan, Y. F., M. E. Marks, F. C. Jones, G. Villarreal Jr., M. D. Shapiro, S. D. Brady, A. M. Southwick, D. M. Absher, J. Grimwood, J. Schmutz, et al. 2010. Adaptive evolution of pelvic reduction in sticklebacks by recurrent deletion of a *Pitx1* enhancer. Science 327:302–305.

Clarke, J. A. 2004. Morphology, phylogenetic taxonomy, and systematics of *Icthyornis* and *Apatornis* (Avialae, Ornithurae) Bull. Am. Mus. Nat. Hist. 286:1–179.

Clarke, J. A., and K. M. Middleton. 2008. Mosaicism, molecules, and the evolution of birds: results from a Bayesian approach to the study of morphological evolution using discrete character data. Syst. Biol. 57:185–201.

Clarke, J. A., Z. Zhou, and F. Zhang. 2006. Insight into the evolution of avian flight from a new clade of Early Cretaceous ornithurines from China and the morphology of *Yixianornis grabaui*. J. Anat. 208:287–308.

Colbert, E. H. 1989. The Triassic dinosaur *Coelophysis*. Mus. N Arizona Bull. 57:1–160.

Compagnucci, C., M. Debiais-Thibaud, M. Coolen, J. Fish, J. N. Griffin, F. Bertocchini, M. Minoux, F. M. Rijli, V. Borday-Birraux, D. Casane, et al. 2013. Pattern and polarity in the development and evolution of the gnathostome jaw: both conservation and heterotopy in the branchial arches of the shark, Scyliorhinus canicula. Dev. Biol. 377:428–448.

Couly, G. F., P. M. Coltey, and N. M. le Douarin. 1993. The triple origin of skull in higher vertebrates: a study in quail-chick chimeras. Development 117:409–429.

Crompton, A. W., and P. Parker. 1978. Evolution of the mammalian masticatory apparatus. Am. Sci. 66:192–201.

Darwin, C. 1859. On the origin of species by means of natural selection. John Murray, London.

Donoghue, M. J. 2005. Key innovations, convergence, and success: macroevolutionary lessons from plant phylogeny. Paleobiology 31:77–93.

Gans, C., and R. G. Northcutt. 1983. Neural crest and the origin of vertebrates: a new head. Science 220:268–274.

Gilbert, S. F. 2010. Developmental biology. 9th ed. Sinauer, Sunderland.

Gill, F. B. 2006. Ornithology. W. H. Freeman, New York.

Gillis, J. A., R. D. Dahn, and N. H. Shubin. 2009. Shared developmental mechanisms pattern the vertebrate gill arch and paired fin skeletons. Proc. Natl. Acad. Sci. 106:5720–5724.

Grant, P. R., and B. R. Grant. 2008. Fission and fusion of Darwin's finch populations. Philos. Trans. R. Soc. Lond. B 363:2821–2829.

Griffin, J. N., C. Compagnucci, D. Hu, J. Fish, O. Klein, R. Marcucio, and M. J. Depew. 2013. Fgf8 dosage determines midfacial integration and polarity within the nasal and optic capsules. Dev. Biol. 374:185–197.

Gussekloo, S. W. S., and R. G. Bout. 2005. Cranial kinesis in paleognathous birds. J. Exp. Biol. 208:3409–3419.

Hanken, J., and D. B. Wake. 1993. Miniaturization of body size: organismal consequences and evolutionary significance. Ann. Rev. Ecol. Syst. 24:501–519.

Heard, S. B., and D. L. Hauser. 1995. Key evolutionary innovations and their ecological mechanisms. Hist. Biol. 10:151–173.

Hennig, W. 1999. Phylogenetic systematics. Univ. Illinois Press, Urbana, IL.

Hödar, C., R. Assar, M. Colombres, A. Aravena, L. Pavez, M. Gonzalez, S. Martinez, N. C. Inestrosa, and A. Maass. 2010. Genome-wide identification of new Wnt/β-catenin target genes in the human genome using CART method. BMC Genom. 11:348.

Hodges, S. A., and M. L. Arnold. 1995. Spurring plant diversification: are floral nectar spurs a key innovation? Proc. R. Soc. B 262:343–348.

Hu, D., and R. S. Marcucio. 2009a. A SHH-responsive signaling center in the forebrain regulates craniofacial morphogenesis via the facial ectoderm. Development 136:107–116.

———. 2009b. Unique organization of the frontonasal ectodermal zone in birds and mammals. Dev. Biol. 325:200–210.

———. 2012. Neural crest cells pattern the surface cephalic ectoderm during FEZ formation. Dev. Dyn. 241:732–740.

Hu, D., R. S. Marcucio, and J. A. Helms. 2003. A zone of frontonasal ectoderm regulates patterning and growth in the face. Development 130:1749–1758.

Hu, Y., and R. C. Albertson. 2014. Hedgehog signaling mediates adaptive variation in a dynamic functional system in the cichlid feeding apparatus. Proc. Natl. Acad. Sci. USA 111:8530–8534.

Jetz, W., G. H. Thomas, J. B. Joy, K. Hartmann, and A. O. Mooers. 2012. The global diversity of birds in space and time. Nature 491:444–448.

Klingenberg, C. P. 2008. Morphological integration and developmental modularity. Ann. Rev. Ecol. Evol. Syst. 39:115–132.

———. 2011. MorphoJ: an integrated software package for geometric morphometrics. Mol. Ecol. Resour. 11:353–357.

Le Douarin, N. M., J. M. Brito, and S. Creuzet. 2007. Role of the neural crest in face and brain development. Brain Res. Rev. 55:237–247.

Lee, M. S., A. Cau, D. Naish, and G. J. Dyke. 2014. Dinosaur evolution. Sustained miniaturization and anatomical innovation in the dinosaurian ancestors of birds. Science 345:562–566.

Lee, S.-H., O. Bedard, M. Buchtova, K. Fu, and J. M. Richman. 2004. A new origin for the maxillary jaw. Dev. Biol. 276:207–224.

Liem, K. F. 1973. Evolutionary strategies and morphological innovations: cichlid pharyngeal jaws. Syst. Zool. 22:425–441.

Lynch, V. J., J. J. Roth, K. Takahashi, C. W. Dunn, D. F. Nonaka, G. F. Stopper, and G. P. Wagner. 2004. Adaptive evolution of HoxA-11 and HoxA-13 at the origin of the uterus in mammals. Proc. Biol. Sci. 271:2201–2207.

Lynch, V. J., A. Tanzer, Y. Wang, F. C. Leung, B. Gellersen, D. Emera, and G. P. Wagner. 2008. Adaptive changes in the transcription factor HoxA-11 are essential for the evolution of pregnancy in mammals. Proc. Natl. Acad. Sci. USA 105:14928–14933.

Lynch, V. J., R. D. Leclerc, G. May, and G. P. Wagner. 2011. Transposon-mediated rewiring of gene regulatory networks contributed to the evolution of pregnancy in mammals. Nat. Genet. 43:1154–1159.

Mallarino, R., and A. Abzhanov. 2012. Paths less traveled: evo-devo approaches to investigating animal morphological evolution. Ann. Rev. Cell Dev. Biol. 28:743–763.

Mallarino, R., P. R. Grant, R. Grant, A. Herrel, W. P. Kuo, and A. Abzhanov. 2011. Two developmental modules establish 3D beak-shape variation in Darwin's finches. Proc. Natl. Acad. Sci. 108:4057–4062.

Marsh, O. C. 1880. Odontornithes: a monograph on the extinct toothed birds of North America—with thirty-four plates and forty woodcuts. US Government Printing Office.

Mayr, G. 2009. Paleogene Fossil Birds. Springer, Heidelberg, Washington, DC.

Mayr, G., and J. Clarke. 2003. The deep divergences of neornithine birds: a phylogenetic analysis of morphological characters. Cladistics 19:527–553.

Noden, D. M. 1978. The control of avian cephalic neural crest cytodifferentiation. I. Skeletal and connective tissues. Dev. Biol. 67:296–312.

Northcutt, R. G. 2011. Evolving large and complex brains. Science 332:926–927.

O'Connor, J. K., and L. M. Chiappe. 2011. A revision of enantiornithine (Aves: Ornithothoraces) skull morphology. J. Syst. Palaeontol. 9:135–157.

O'connor, J. K., and Z. H. Zhou. 2013. A redescription of Chaoyangia beishanensis (Aves) and a comprehensive phylogeny of Mesozoic birds. J. Syst. Palaeontol. 11:889–906.

Parsons, K. J., A. T. Taylor, K. E. Powder, and R. C. Albertson. 2014. Wnt signalling underlies the evolution of new phenotypes and craniofacial variability in Lake Malawi cichlids. Nat. Commun. 5:3629.

Patterson, C. 1982. Morphological characters and homology. Pp. 21–74 *in* K. A. Joysey, and A. E. Friday, eds. Problems of phylogenetic reconstruction. Academic Press, London/New York.

Reid, B. S., H. Yang, V. S. Melvin, M. M. Taketo, and T. Williams. 2011. Ectodermal Wnt/beta-catenin signaling shapes the mouse face. Dev. Biol. 349:261–269.

Romer, A. S., and T. S. Parsons. 1990. The Vertebrate Body. Saunders College Publishing, Fort Worth, TX.

Shapiro, M. D., M. E. Marks, C. L. Peichel, B. K. Blackman, K. S. Nereng, B. Jónsson, D. Schluter, and D. M. Kingsley. 2004. Genetic and developmental basis of evolutionary pelvic reduction in threespine sticklebacks. Nature 428:717–723.

Shubin, N., C. Tabin, and S. Carroll. 2009. Deep homology and the origins of evolutionary novelty. Nature 457:818–823.

Simpson, G. G. 1953. The major features of evolution. Columbia Univ. Press, New York.

Wada, N., T. Nohno, and S. Kuratani. 2011. Dual origins of the prechordal cranium in the chicken embryo. Dev. Biol. 356:529–540.

Wagner, G. P. 2014. Homology, genes, and evolutionary innovation. Princeton Univ. Press, Princeton, NJ.

Wagner, G. P., and V. J. Lynch. 2010. Evolutionary novelties. Curr. Biol. 20:R48–R52.

Warren, S. M., L. J. Brunet, R. M. Harland, c. A. N., and M. T. Longaker. 2003. The BMP antagonist noggin regulates cranial suture fusion. Nature 422:625–629.

Young, N. M., D. Hu, A. J. Lainoff, F. J. Smith, R. Diaz, A. S. Tucker, P. A. Trainor, R. A. Schneider, B. Hallgrimsson, and R. S. Marcucio. 2014. Embryonic bauplans and the developmental origins of facial diversity and constraint. Development 141:1059–1063.

Zhou, S., Z. Zhou, and J. K. O'Connor. 2013. Anatomy of the basal ornithuromorph bird *Archaeorhynchus spathula* from the Early Cretaceous of Liaoning, China. J. Vertebr. Paleontol. 33:141–152.

Zhou, Z., and F. Z. Z. Li. 2010. A new Lower Cretaceous bird from China and tooth reduction in early avian evolution. Proc. R. Soc. B 277:219–227.

Associate Editor: C. Wheat
Handling Editor: R. Shaw

Supporting Information

Additional Supporting Information may be found in the online version of this article at the publisher's website:

Figure S1. Cell death and proliferation at HH equivalent 24-26.
Figure S2. Phylogenetic structure of PCAs.
Figure S3. Strong phenotype from WNT inhibitor IWR-1, E18.
Figure S4. The palatines (in red) of normal chickens at early stages of ossification already have the bird-specific narrow and anteriorly directed phenotype.
Figure S5. Results of Fgf-inhibition experiments on forelimb buds.

A molecular mechanism for the origin of a key evolutionary innovation, the bird beak and palate, revealed by an integrative approach to major transitions in vertebrate history

Bhart-Anjan S. Bhullar, Zachary S. Morris, Elizabeth M. Sefton, Atalay Tok, Masayoshi Tokita, Bumjin Namkoong, Jasmin Camacho, David A. Burnham & Arhat Abzhanov

Supplementary Information

Table of Contents

Supplementary Data 1. PCA methods and analyses

Landmarks were digitized with tpsDIG v2.16(Rohlf 2005) and sliding semilandmarks specified using TPSUtil; Procrustes alignment and principal component analysis were performed in TPSRelW and MorphoJ(Klingenberg 2011). The procedures were performed as described previously(Bhullar et al. 2012). Phylogenies for phylogenetic mapping were derived from references used in previous work(Bhullar et al. 2012) and recent systematic analyses(O'connor

and Zhou 2013). Phylogenetic mapping and permutation tests for phylogenetic signal were performed in MorphoJ using the rooted tree option and 70,000 iterations. Visualizations of the phylogenetic mapping are provided in Fig. S2. Partial least squares was performed by matching the premaxillae and palatines of individuals using two-block PLS in MorphoJ and a permutation test with 70,000 rounds. PCA Landmarks and specimens used are described in the following sections.

Supplementary Data 2. Specimen list for PCA data

Sources are dorsal and palatal figures as listed previously(Bhullar et al. 2012) and duplicated below with the following additions:

Archaeorhychus spathula. Published photographs(Zhou et al. 2013)

Gobipteryx minuta. Published photographs(Chiappe et al. 2001).

Hesperornis regalis. New CT scans of specimen KUVP (University of Kansas Vertebrate Paleontology Collection) 71012

Saurosuchus galilei PVSJ (Museo de Ciencias Naturales, Universidad Nacional de San Juan, Argentina) 32. From UTCT data. URL http://digimorph.org/specimens/Saurosuchus_galilei/

Saurornithoides mongoliensis AMNH (American Museum of Natural History) FR 6516. From UTCT data. URL http://digimorph.org/specimens/Saurornithoides_mongoliensis/

Sources from previous work:
Non-dinosaur outgroups:

Euparkeria capensis. Published reconstruction(Ewer 1965).

Alligator mississippiensis E46. Uncatalogued specimen, μCT scanned at Harvard Center for Nanoscale Systems with X-Tek Model HMXST225. Copper target, 80 kV, 95 μA, 1.5 second exposure time with a -27 focus setting. Scanned with two samples per view and hardware ring artifact correction.

Primitive theropods:

Eoraptor lunensis. Specimen PVSJ (Museo de Ciencias Naturales, Universidad Nacional de San Juan, Argentina) 512. From UTCT data. URL: http://digimorph.org/specimens/Eoraptor_lunensis/

Herrerasaurus ischigualastensis adult. Published reconstruction(Sereno and Novas 1993).

Coelophysis bauri adult. Photograph of specimen MCZ 4327.

Intermediate-grade theropods:

Ceratosaurus nasicornis adult. Published reconstruction(Paul 1988).

Majungasaurus crenatissimus adult. Published CT image(Sampson and Witmer 2007).

Suchomimus tenerensis adult. Published reconstruction(Sereno et al. 1998).

Allosaurus fragilis adult. Published reconstruction(Madsen 1976).

Non-maniraptoran coelurosaurs:

Guanlong wucaii adult. Published reconstruction(Xu et al. 2006).

Dilong paradoxus adult. Published reconstruction(Xu et al. 2004).

Gorgosaurus libratus adult. Published drawing(Currie et al. 2003).

Tarbosaurus bataar juvenile. Published CT image(Tsuihiji et al. 2011).

Tarbosaurus bataar adult. Published drawing(Hurum and Sabath 2003).

Tyrannosaurus rex subadult, adult, and large adult. Published reconstructions(Carr 1999).

Non-eumaniraptoran maniraptorans:

Garudimimus brevipes adult. Published photograph(Kobayashi and Barsbold 2005).

Haplocheirus sollers adult. Photograph of holotype, IVPP (Institute of Vertebrate Paleontology and Paleoanthropology, Chinese Academy of Science, Beijing) V 15988(Choiniere et al. 2010).

Erlicosaurus andrewsi adult. Published photograph(Clark et al. 1994).

Incisivosaurus gauthieri adult. Specimen IVPP V 13326. From UTCT data. URL: http://digimorph.org/specimens/Incisivosaurus_gauthieri/

Citipati osmolskae adult. Published photograph(Clark et al. 2002).

Non-avian eumaniraptorans:

Bambiraptor feinbergi. Published reconstruction(Burnham et al. 2000).

Velociraptor mongoliensis adult. Photograph of specimen IGM (Institute of Geology, Mongolian Academy of Sciences, Ulaan Baator) 100/25.

Zanabazar junior adult. Published reconstruction(Norell et al. 2009).

Byronosaurus perinate. Novel reconstruction from photograph of specimen IGM 100/974(Bever and Norell 2009).

Byronosaurus jaffei adult. Novel reconstruction based on UTCT data of specimen IGM 100/983. URLs: http://digimorph.org/specimens/Byronosaurus_jaffei/rostrum/, http://digimorph.org/specimens/Byronosaurus_jaffei/braincase/

Archaeopteryx adult. Photograph of Thermopolis specimen.

Confuciusornis sanctus adult. Photograph of specimen GMV (National Geological Museum of China, Beijing) 2132.

Yixianornis grabaui adult. Composite reconstruction based on published and unpublished photographs of *Yixianornis*(Clarke et al. 2006), *Aberratiodontus wui*(Gong et al. 2004), and *Yanornis martini*.

Aves:

Eudromia sp. adult. Photograph of uncatalogued specimen.

Gallus gallus adult. Specimen TMM M-1545. From UTCT data. URL: http://digimorph.org/specimens/Gallus_gallus/adult/

Scan data are available by request from The University of Texas High-Resolution X-Ray Computed Tomography Facility (UTCT).

Supplementary Data 3. Parsimony analysis

Gene expression characters were scored in Mesquite v. 2.75(Maddison and Maddison 2011). The ancestral state reconstruction package under the default parsimony model was used to reconstruct the states at nodes in the tree as shown in Fig. 2b.

Supplementary Data 4. Embryo collection and in-situ hybridization materials and methods

Chicken eggs were acquired from the University of Connecticut and incubated to the appropriate ages. Alligator eggs were collected from Rockefeller Wildlife Refuge, Louisiana Department of Wildlife and Fisheries, and incubated in humidified incubators until collection. Emu eggs were incubated at Songline Emu Farm, Gill, Massachusetts until the requested ages and then collected there. All embryos were dissected out of the eggs, washed in phosphate-buffered saline solution, and fixed in 4% paraformaldehyde overnight before being stored at -20° C in 100% methanol.

cDNA libraries were constructed using the New England Biolabs Protoscript M-MulV First Strand cDNA Synthesis Kit. Gene fragments were amplified and cloned from cDNA with RT-PCR using the following primers: Emu *Fgf8* f 5' TACACTCCCTCGTCTCGGAC 3' and r 5' GCCCTTGCGGGTGAAGGCCA 3'; Emu and alligator *Lef1* f 5' CGAACATGTCGTTCCCTGGTA 3' r 5' GGGCCTGTACCTGATGCTGATT 3'; Alligator *Fgf8* f 5' TACACTCCCTCGTCTCGG 3' r 5' CCCTTGCGGGTGAAGGCCATG 3'; Anole *Fgf8* f 5' CTCGTTACCCTTTCCGTT 3' r 5' TACAGCTGATAGGTGCGGAC 3'; Alligator *Shh* f 5' GAGTGGGGGTTAATGTTG 3' 4 5' CTGCAGCAGGCGGGCTCGC 3'. Riboprobes were created and whole-mount and section *in-situ* hybridization was performed as described previously(Brent et al. 2003). Alligator probes were used to visualize turtle gene expression.

Supplementary Data 5. Functional experiment materials and methods

All functional experiments began with chick eggs incubated at 38 degrees Celsius and 50-80% humidity. At Embryonic Day 2, 4 mL of albumin was removed using a syringe in order to lower the yolk and make the embryos ready for manipulation.

Eggs were incubated until HH stage 18 for FGF facial inhibition experiments and until HH 24 for FGF limb bud inhibition experiments and for WNT facial inhibition experiments. At these stages, their surfaces were reinforced using packing tape and oval windows ~2 cm in diameter were cut in them with small scissors just prior to manipulation.

Fine forceps were used to remove the external membrane from the surfaces of the embryos in the region of manipulation. Custom-made tungsten needles made by flame-sharpening tungsten wire, mounted in glass handles made from capillary tubes, were used as dissection tools to cut slits for bead implantation. The needles were sterilized after each operation. For facial implantation, superficial slits were cut precisely in the midline of the frontonasal prominence and beads implanted within them such that the beads were held in place in the epithelium and did not fall out or fall inward to the mesenchyme or brain cavity. For limb bud implantation, superficial slits were cut in the region of the apical ectodermal ridge and beads implanted in these by gripping and inserting them with very fine forceps.

The ion exchange beads used were formate-derivatized AG1-X2 from BioRad.. All chemicals were dissolved in DMSO and control beads were soaked with DMSO (Sigma) lacking chemical but otherwise treated identically and implanted in alternating sequence with the experimental beads during the same experiments. Soaking was accomplished by placing a 20 uL droplet of fluid on a piece of Parafilm within a small plastic petri dish, then transferring dried beads to the droplet and leaving at room temperature for 3 hours. The beads were then transferred to a small tube containing PBS and rinsed in this way twice. For introduction of beads into the egg, a pipette was used and extra beads were lifted out of the eggs using needles and forceps. After operation, eggs were resealed with tape and placed back into the incubator after a resting period of approximately 15 minutes at room temperature.

The SU5402 (Calbiochem), fibroblast growth factor receptor (FGFR) inhibitor, was used at concentrations of 5, 1, and 0.33 mM. The PD98059 (Calbiochem) is a highly selective noncompetitive inhibitor of MEK1 and MEK2 and prevents the activation of MAPKK1 by Raf or MEK kinase downstream of FGF pathway. The PD98059 was used at a concentration of 1 mM to confirm Fgf involvement. The WNT antagonists FH535 (Calbiochem) and IWR-1 (Sigma) used at a concentration of 5 mM. Embryos were collected upon death, at E15 (to maximize survival of experimentals, which underwent a bottleneck after this stage), and at E19 (near-hatching). They were fixed in 4% paraformaldehyde and stored in 70% ethanol in PBS. For CT scanning, they were rehydrated to PBS to avoid desiccation during the scanning process.

Supplementary Data 6. Summary of functional experiment effects

Facial phenotypes were visible as early as E10 but ossification sufficient to include in the morphometric analysis was not present until E18. Embryos treated with 5 mM SU5402 died by E15 and had severely truncated upper jaws as reported previously with 10 mM SU5402(Hu and Marcucio 2012). Of the embryos treated with 1 mM su5402, 13/18 showed phenotypes and 4 of these were strong phenotypes as depicted in Fig. 4. Of the embryos treated with 0.33 mM SU5402, 17/25 showed phenotypes and all were mild. 0/43 control embryos during su5402 experiments showed phenotypes. Of the embryos treated with 1 mM PD98059, 4/5 showed phenotypes and 1 of these was strong. 0/6 control embryos during these experiments showed phenotypes. Of the embryos treated with 5 mM FH535, 5/7 showed phenotypes and 1 of these was strong. 0/8 control embryos during these experiments showed phenotypes. Of the embryos treated with 5 mM IWR-1, 3/4 showed phenotypes and 1 of these was strong. 0/5 control animals during these experiments showed phenotypes.

The facial phenotypes, whether strong or mild, were notable in the localization of the modifications to the premaxilla (Fig. S3), with slight accommodating broadening of the nasals and frontals. Other regions of the skull were normal, as expected because only the frontonasal prominence was altered.

In addition to the facial experiments, both FGF inhibitors were tested by a small number of unilateral implantations into the AER of HH stage 24 forelimb buds, where they would be expected to inhibit FGF-mediated limb outgrowth and result in a distally truncated limb phenotype. 2/4 surviving experimental animals implanted with 5 mM SU5402 beads and 1/3 experimental embryos implanted with 5 mM PD98059 beads displayed the expected limb truncations on the right (implanted) sides but not the left (Fig. S5). Of these, one of the su5402-implanted embryos showed absence of the autopod and zeugopod, leaving only a partial stylopod (humerus) (Fig. S5a, d-g). The other two embryos showed absence of the autopod and the distal zeugopod but retained a humerus and a partial radius and ulna (Fig. S5b-c, h-k). Moreover, 0/10 animals implanted with control beads showed limb malformations.

Supplementary Data 7: Cell death and proliferation assays

Cell death assays were performed using a commercially available TUNEL kit (Roche, AP TUNEL Detection Kit) with no modifications to the protocol. Images were taken using a fluorescence microscope directly after the first TUNEL reaction. Proliferation was detected using a rabbit phospho-histone H3 (Ser10 residue) antibody (Cell Signaling Technologies) as described in an open online resource (Ryan Rountree, 2002, http://kingsley.stanford.edu/Lab%20Protocols-WEB%202003/Molecular%20Biology/Cell_Death=TUNEL_&_prolif.htm) using a fluorescent goat-anti-rabbit secondary antibody.

Supplementary Data 8. Supplementary figures

FIGURE S1

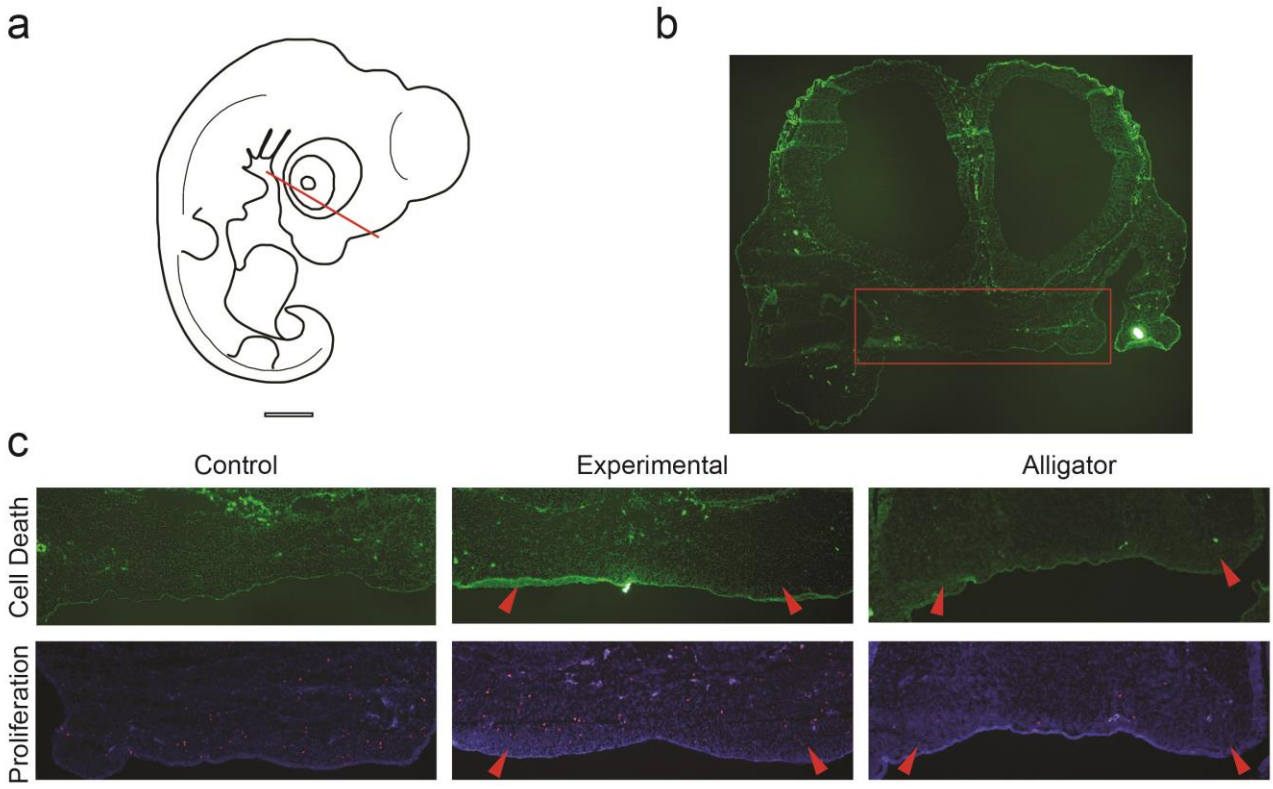

Figure S1. Cell death and proliferation at HH equivalent 24-26. a, Approximate plate of section. **b,** Area of magnification shown in control chick cell death assay; note considerable amounts of cell death around periphery of brain. **c,** Cell death and proliferation in control and experimental chicks and alligator. Red arrows indicate bilateral regions of outgrowth present in experimental chick and alligator. Scale bar is 100 μm.

FIGURE S2

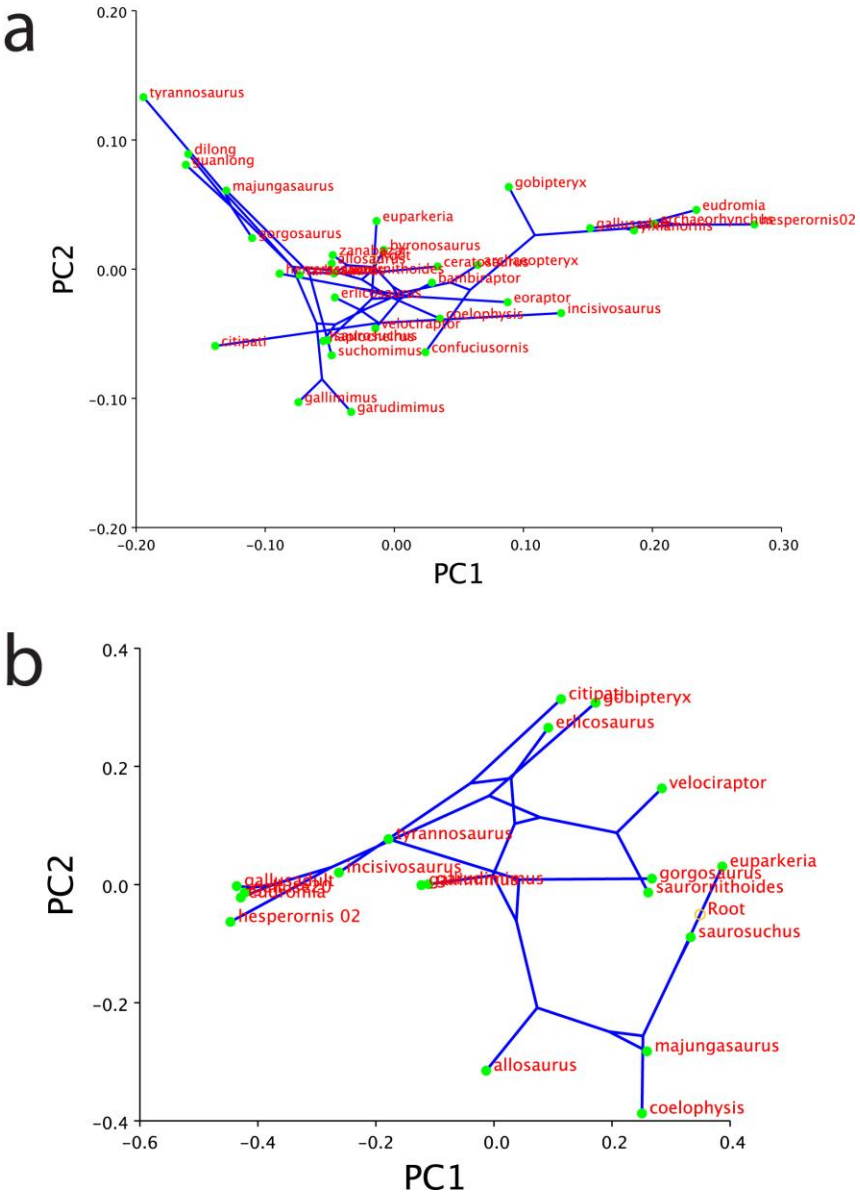

Figure S2. Phylogenetic structure of PCAs. a, Premaxilla. **b,** Palatine.

FIGURE S3

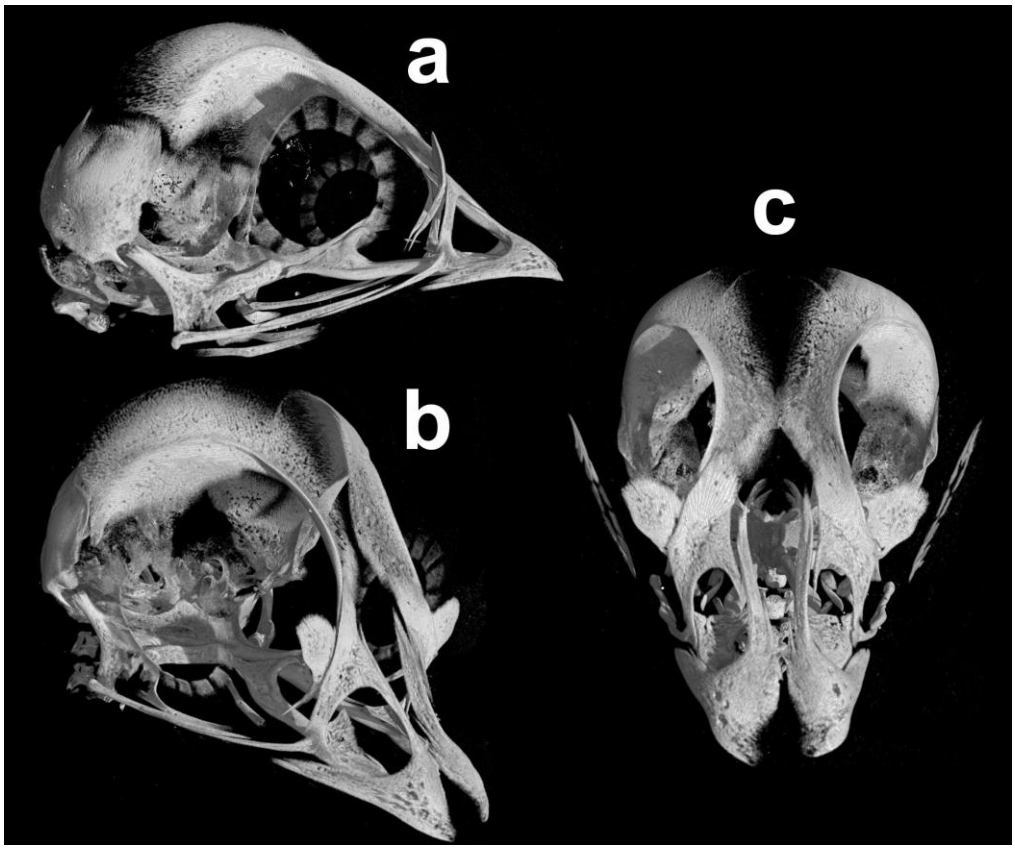

Figure S3. Strong WNT phenotype resulting from experiments with IWR-1 inhibitor, E18. a, Right lateral. **b,** Oblique anterolateral. **c,** Anterodorsal.

FIGURE S4

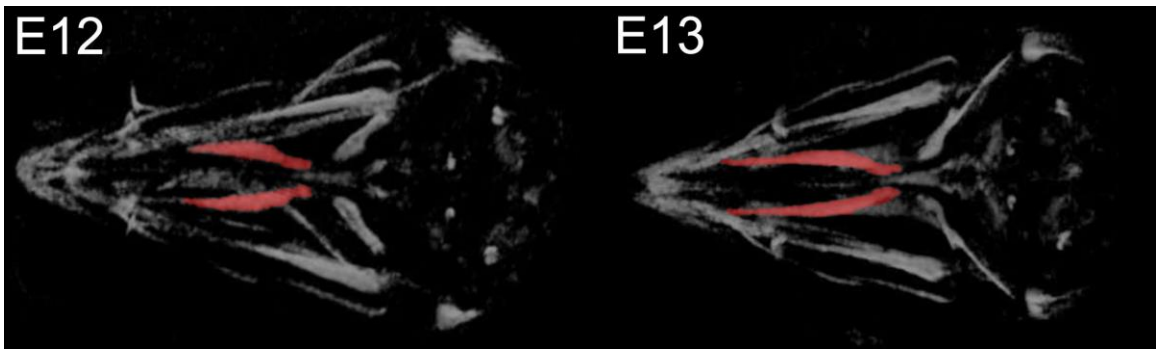

Figure S4. The palatines (in red) of normal chickens at early stages of ossification already have the bird-specific narrow and anteriorly directed phenotype. Modified after data from UTCT/www.digimorph.org

FIGURE S5

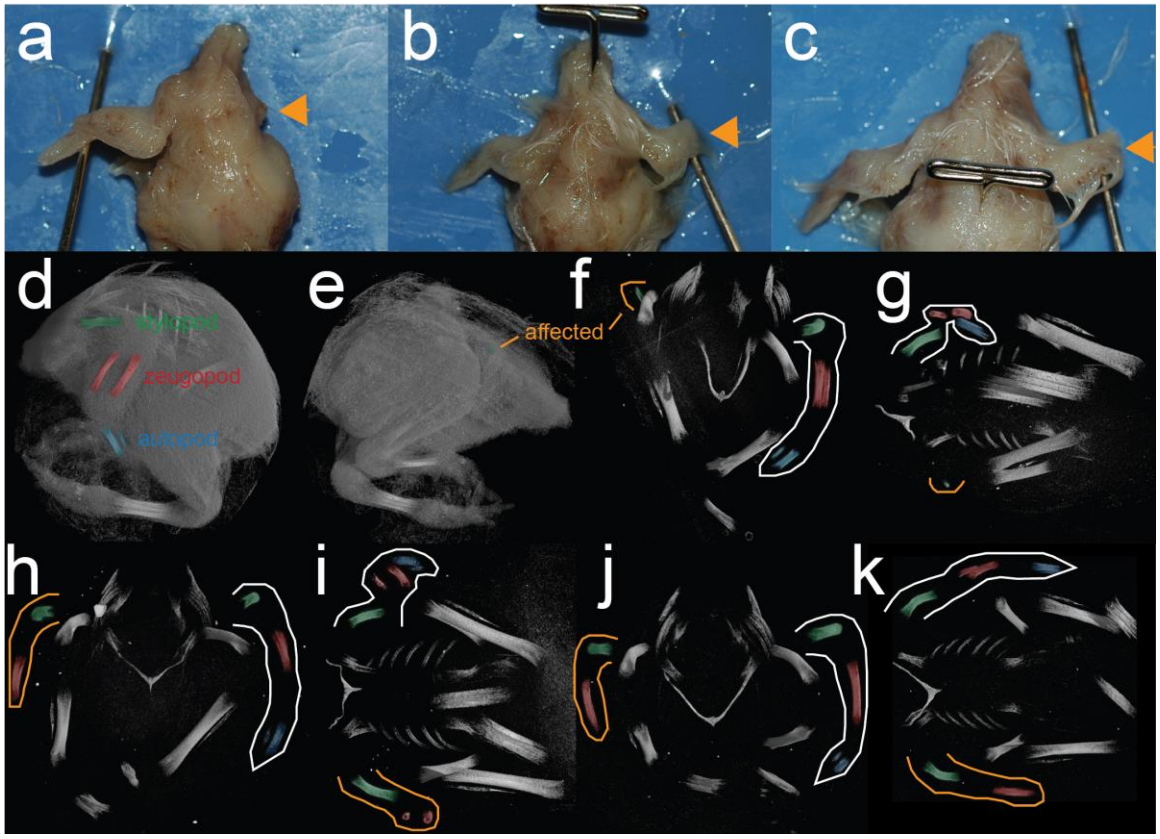

Figure S5. Results of FGF-inhibition experiments on forelimb buds. a, External view of SU5402 strong phenotype, with only remnant stylopod remaining on affected (right) side. **b,** External view of SU5402 moderate phenotype, with autopod truncated. **c,** External view of PD98059 phenotype with autopod truncated. **d,** Unaffected side of SU5402 strong phenotype showing stylopod in green, zeugopod in red, and autopod in blue. **e,** Affected side of SU5402 strong phenotype showing remnant of stylopod. **f,** Anterior view of skeleton of SU5402 strong phenotype, affected forelimb outlined in orange showing severe truncation of entire limb. **g,** Ventral view of skeleton of SU5402 strong phenotype. **h,** Anterior view of skeleton of SU5402 moderate phenotype showing absence of autopod. **i,** Ventral view of skeleton of SU5402 moderate phenotype. **j,** Anterior view of skeleton of PD98059 phenotype showing absence of autopod. **h,** Ventral view of skeleton of PD98059 phenotype.

Supplementary Data 9. References

Bever, G. S. and M. A. Norell. 2009. The perinate skull of *Byronosaurus* (Troodontidae) with observations on the cranial ontogeny of paravian theropods. American Museum Novitates 3657:1-51.

Bhullar, B.-A. S., J. Marugan-Lobon, F. Racimo, G. S. Bever, T. B. Rowe, M. A. Norell, and A. Abzhanov. 2012. Birds have paedomorphic dinosaur skulls. Nature 487:223-226.

Brent, A. E., R. Schweitzer, and C. J. Tabin. 2003. A somitic compartment of tendon progenitors. Cell 113:235-248.

Burnham, D. A., K. L. Derstler, P. J. Currie, R. T. Bakker, Z. Zhou, and J. H. Ostrom. 2000. Remarkable new birdlike dinosaur (Theropoda: Maniraptora) from the Upper Cretaceous of Montana. University of Kansas Paleontological Contributions 13:1-14.

Carr, T. D. 1999. Craniofacial ontogeny in Tyrannosauridae (Dinosauria, Coelurosauria). Journal of Vertebrate Paleontology 19:497-520.

Chiappe, L. M., M. Norell, and J. Clark. 2001. A new skull of *Gobipteryx minuta* (Aves: Enantiornithes) from the Cretaceous of the Gobi Desert. American Museum Novitates 3346:1-15.

Choiniere, J. N., X. Xu, J. M. Clark, C. A. Forster, Y. Guo, and F. Han. 2010. A basal alvarezsauroid theropod from the Early Late Jurassic of Xinjiang, China. Science 327:571-574.

Clark, J. M., P. Altangerel, and M. A. Norell. 1994. The skull of *Erlicosaurus andrewsi*, a Late Cretaceous "segnosaur" (Theropoda: Therizinosauridae) from Mongolia. American Museum Novitates 3115:1-39.

Clark, J. M., M. A. Norell, and T. Rowe. 2002. Cranial anatomy of *Citipati osmolskae* (Theropoda, Oviraptorosauria), and a reinterpretation of the holotype of *Oviraptor philoceratops*. American Museum Novitates 3364:1-24.

Clarke, J. A., Z. Zhou, and F. Zhang. 2006. Insight into the evolution of avian flight from a new clade of Early Cretaceous ornithurines from China and the morphology of *Yixianornis grabaui*. Journal of Anatomy 208:287-308.

Currie, P. J., J. H. Hurum, and K. Sabath. 2003. Skull structure and evolution in tyrannosaurid dinosaurs. Palaeontologia Polonica 48:227-234.

Ewer, R. F. 1965. The anatomy of the thecodont reptile *Euparkeria capensis* Broom. Philosophial Trasactions of the Royal Society of London. Series B. 248:379-435.

Gong, E., L. Hou, and L. Wang. 2004. Enantiornithine bird with diapsidan skull and its dental development in the Early Cretaceous in Liaoning, China. Acta Geologica Sinica 78:1-7.

Hu, D. and R. S. Marcucio. 2012. Neural crest cells pattern the surface cephalic ectoderm during FEZ formation. Developmental Dynamics 241:732-740.

Hurum, J. H. and K. Sabath. 2003. Giant theropod dinosaurs from Asia and North America: Skulls of *Tarbosaurus bataar* and *Tyrannosaurus rex* compared. Palaeontologia Polonica 48:161-190.

Klingenberg, C. P. 2011. MorphoJ: an integrated software package for geometric morphometrics. Molecular Ecology Resources 11:353-357.

Kobayashi, Y. and R. Barsbold. 2005. Reexamination of a primitive ornithomimosaur, *Garudimimus brevipes* Barsbold, 1981 (Dinosauria: Theropoda), from the Late Cretaceous of Mongolia. Canadian Journal of Earth Science 42:1501-1521.

Maddison, W. P. and D. R. Maddison. 2011. Mesquite: a modular system for evolutionary analysis. Version 2.75.

Madsen, J. H. 1976. *Allosaurus fragilis*: a revised osteology. Utah Geological and Mineral Survey Bulletin 109:1-163.

Norell, M. A., P. J. Makovicky, G. S. Bever, A. M. Balanoff, J. M. Clark, R. Barsbold, and T. Rowe. 2009. A review of the Mongolian Cretaceous dinosaur *Saurornithoides* (Troodontidae: Theropoda). American Museum Novitates 3654:1-63.

O'connor, J. K. and Z. H. Zhou. 2013. A redescription of Chaoyangia beishanensis (Aves) and a comprehensive phylogeny of Mesozoic birds. Journal of Systematic Palaeontology 11:889-906.

Paul, G. S. 1988. Predatory Dinosaurs of the World: A Complete Illustrated Guide. Simon and Schuster, New York.

Rohlf, F. J. 2005. tpsDig, digitize landmarks and outlines. Department of Ecology and Evolution, State University of New York at Stony Brook.

Sampson, S. D. and L. M. Witmer. 2007. Craniofacial anatomy of *Majungasaurus crenatissimus* (Theropoda: Abelisauridae) from the Late Cretaceous of Madagascar. Journal of Vertebrate Paleontology 27:S2:32-104.

Sereno, P. C., A. L. Beck, D. B. Dutheil, B. Gado, H. C. E. Larsson, G. H. Lyon, J. D. Marcot, O. W. M. Rauhut, R. W. Sadleir, C. A. Sidor, D. D. Varricchio, G. P. Wilson, and J. A. Wilson. 1998. A long-snouted predatory dinosaur from Africa and the evolution of spinosaurids. Science 282:1298-1302.

Sereno, P. C. and F. E. Novas. 1993. The skull and neck of the basal theropod *Herrerasaurus ischigualastensis*. Journal of Vertebrate Paleontology 13:451-476.

Tsuihiji, T., M. Watabe, K. Togtbaatar, T. Tsubamoto, R. Barsbold, S. Suzuki, A. H. Lee, R. C. Ridgely, Y. Kawahara, and L. M. Witmer. 2011. Cranial osteology of a juvenile specimen of *Tarbosaurus bataar* (Theropoda, Tyrannosauridae) from the Nemegt Formation (upper Cretaceous) of Bugin Tsav, Mongolia. Journal of Vertebrate Paleontology 31:1-21.

Xu, X., J. M. Clark, C. A. Forster, M. A. Norell, G. M. Erickson, D. A. Eberth, C. Jia, and Q. Zhao. 2006. A basal tyrannosauroid dinosaur from the Late Jurassic of China. Nature 439:715-718.

Xu, X., M. A. Norell, X. Kuang, X. Wang, Q. Zhao, and C. Jia. 2004. Basal tyrannosauroids from China and evidence for protofeathers in tyrannosauroids. Nature 431:680-684.

Zhou, S., Z. Zhou, and J. K. O'Connor. 2013. Anatomy of the basal ornithuromorph bird *Archaeorhynchus spathula* from the Early Cretaceous of Liaoning, China. Journal of Vertebrate Paleontology 33:141-152.